RHEINISCH-
WESTFÄLISCHE
TECHNISCHE
HOCHSCHULE
AACHEN

Institute of Flight System
Dynamics
Univ.-Prof. Dr.-Ing. D. Moormann

Diploma Thesis

An Investigation of Glider Winch Launch Accidents Utilizing Multipoint Aerodynamics Models in Flight Simulation

cand. ing. Christoph G. Santel

December 2, 2010

communicated by Univ.-Prof. Dr.-Ing. D. Moormann

Advising Tutor: Dipl.-Ing. Andreas Gäb

Aufgabenstellung

Untersuchungen zum Kontrollverlust von Segelflugzeugen im Windenstart mittels Mehrpunktaerodynamik-Modelle in der Flugsimulation

Die häufigste Startart für Segelflugzeuge in Deutschland ist der Windenstart. Obwohl dieser insgesamt als sehr sicher anzusehen ist, geschehen dabei immer noch Unfälle. Ein besonders kritischer Bereich beim Windenstart ist der Anfangssteigflug, in dem es immer wieder zum Abkippen oder Durchsacken des Segelflugzeugs kommt. Es wird vermutet, dass diese Effekte mit der sogennanten "Aufbäumneigung" des Flugzeugs sowie dem "dynamischem Überziehen" zusammenhängen.

Im Rahmen dieser Diplomarbeit soll ein derartiges Flugverhalten reproduziert werden. Das bestehende Simulationswerkzeug des Lehrstuhls soll um ein geeignetes Aerodynamik-Modell ergänzt werden. Mittels dieser Modelle sollen tatsächliche Unfallverläufe nachgestellt und diskutiert werden. Die Beschaffung des Datensatzes für ein repräsentatives Flugzeugmuster ist ebenfalls Bestandteil der Aufgabe und notwendig für die Unfallnachstellung.

Folgende Arbeitsschritte sind durchzuführen:

- Statistische Auswertung der BFU-Datenbanken zu Windenstartunfällen – 1 Woche
- Erweiterung des Simulationswerkzeugs und Modellbildung – 7 Wochen
- Beschaffung des Datensatzes eines repräsentativen Flugzeugmusters – 2 Wochen
- Validierung und Plausibilitätsüberprüfung der implementierten Modelle – 2 Wochen
- Durchführung und Auswertung von Analysen zu Windenstartunfällen – 2 Wochen
- Ausführliche Dokumentation aller Arbeitspunkte – 3 Wochen

Task

An Investigation of Glider Winch Launch Accidents Utilizing Multipoint Aerodynamics Models in Flight Simulation

Winch launching is the most frequently used method of launching sailplanes in Germany. Even though this is considered as a relatively safe method of launching, accidents still occur. The initial climb phase is particularly critical. In the past, aircraft have lost lift and begun to roll inverted during this phase. A common hypothesis is that this is linked to the aircraft's "pitch-up" tendency and "dynamic stall" effects.

It shall be attempted to recreate this behavior within the frame of the thesis. The *Institute of Flight System Dynamics*' simulation tool shall be supplemented with appropriate aerodynamics models. Accidents shall be recreated and discussed by making use of these models. Obtaining a dataset of a representative aircraft model is also part of this thesis and necessary for accident reconstruction.

The following steps are to be completed within the frame of this thesis:

- Statistical analysis of winch launch accidents from the BFU database – 1 week
- Extension of the simulation tool and modeling – 7 weeks
- Obtaining the dataset of a representative aircraft model – 2 weeks
- Validation and checks of plausibility of the models implemented – 2 weeks
- Realization and discussion of analyses of winch launch accidents – 2 weeks
- Comprehensive documentation of all work done – 3 weeks

Contents

List of Figures

List of Tables

List of Symbols

Notation	
C	Coefficient
D	Drag
D'	Panel Drag
E	Glide Ratio
$\boldsymbol{I}$	Inertial Tensor
I	Moment of Inertia
L'	Panel Lift
$\boldsymbol{M}$	Matrix of Rotation
$\vec{M}$	Moment
M'	Panel Moment
N	Absolute Number of Accidents
P	Absolute Number of Persons Injured
Re	Reynolds Number
S	Area
$\vec{V}$	Vectorial Velocity
V	Scalar Velocity
	Volume
a	Average Number of Persons Injured
b	Width
c	Chord
f	Frequency
g	Gravitational Acceleration
h	Shortest Distance Between Vortex Axis and Evaluation Point
	Height above Ground
i	Angle of Incidence
	Index of Specified Item
k	Correction Factor
	Multiple
m	Mass
n	Relative Number of Accidents
	Total Number of Specified Item
	Load Factor
p	Probability of Injury
	Pressure
p, q, r	Cartesian Rotational Velocity Components
$\vec{r}$	Location Vector

continued on next page

r	Radius
t	Time
u, v, w	Cartesian Translational Velocity Components
$\vec{x}$, $\vec{y}$, $\vec{z}$	Cartesian Coordinate Axes
Δ	Discrete Difference
Λ	Aspect Ratio
Θ	Pitch Angle
$\vec{\Omega}$	Vector of Rotational Speed
α	Angle of Attack
$\dot{\alpha}^\star$	Non-dimensional Temporal Derivative of Angle of Attack
β	Angle of Sideslip
γ	Climb Angle
δ	Control Surface Deflection Angle
ε	Convergence Parameter
	Downwash Angle
ζ	Angle from Vortex Element to Evaluation Point
	Rudder Pedal Displacement
η	Longitudinal Control Stick Displacement
κ	Flap Control Handle Setting
λ	Angle between Glider's Longitudinal Axis and Cable Force
μ	Dynamic Viscosity of Air
ν	Angle of Dihedral
ξ	Lateral Control Stick Displacement
ρ	Air Density
ϕ	Lead Angle
φ	Angle of Sweep

Indices

A	Aerodynamic Parameter
a	Global Aerodynamic Coordinates
	Aileron
AC	Aerodynamic Center
C	Cable
CG	Center of Gravity
CG-Hook	Center of Gravity Tow Hook
circ	Circulation
conv	Convergence
crit	Critical
dyn	Dynamic
D	Drag
D'	Panel Drag
d	Airfoil Drag

continued on next page

dw	Downwash
e	Elevator
eff	Effective
eval	Evaluation
f	Fatal Injury,
	Aircraft Body-fixed Coordinates
fade	Fading
fu	Fuselage
g	Global Earth-fixed Coordinates
	Gyration
GCP	Ground Contact Point
ge	Ground Effect
geo	Geometric
h	Horizontal Stabilizer
i	Index of Launch Phase
IGE	In Ground Effect
k	Flap
L	Lift
L'	Panel Lift
l	Airfoil Lift
	Left-Hand Side
LG	Landing Gear
ll	Lifting Line
ls	Lifting Surfaces
M	Pitching Moment
M'	Panel Moment
m	Minor Injury
	Airfoil Moment
mw	Main Wing
mac	Mean Aerodynamic Chord
max	Maximum
min	Minimum
mp	Mirror Plane
N	Yawing Moment
n	No Injury
OGE	Out of Ground Effect
p	Panel-fixed Coordinates
pan	Panel
pcp	Panel Center Point
proj	Projected
r	Rudder
	Right-Hand Side
ref	Reference
release	Release
S	Stall
s	Severe Injury,

continued on next page

	Structural Coordinates
sec	Vortex Section
stat	Static
surf	Lifting Surface
W	Winch Launch
wsp	Wake Support Point
x, y, z	Cartesian Coordinate Axes
Y	Side Force
0	Zero-Lift Condition

Abbreviations

6DoF	six Degrees of Freedom
AC	Aerodynamic Center
BET	Blade Element Theory
BFU	German Federal Bureau of Aircraft Accident Investigation ("Bundesstelle für Flugunfalluntersuchung")
CG	Center of Gravity
IGE	In Ground Effect
ISA	International Standard Atmosphere
NASA	National Aeronautics and Space Administration
OGE	Out of Ground Effect
TMG	Touring Motorglider

Conventions in Mathematical Notation

Z	Scalar Term, Absolute Value of $\vec{Z}$
$\dot{Z}$	Temporal Derivative of Z
$\vec{Z}$	Vector Z
$\boldsymbol{Z}$	Matrix Z
$\lceil Z \rceil$	Ceiling Function of Z
$\tilde{\vec{Z}}$	Vector $\vec{Z}$ Mirrored
$\vec{Y} \times \vec{Z}$	Cross Product of Vectors $\vec{Y}$ and $\vec{Z}$
$\angle \vec{Y}, \vec{Z}$	Intersecting Angle of Vectors $\vec{Y}$ and $\vec{Z}$
$Y \vee Z$	Y or Z

Typeset Conventions

`Typewriter`	Name of m-File, Function or Block

Abstract

The presented thesis investigated the mechanisms leading to accidents during the winch launch of gliders. Initially, data from the accident database of the *German Federal Bureau of Aircraft Accident Investigation* was studied. Critical phases of the launch were identified along with the associated probabilities and risks of accidents. From this data requirements to an aerodynamics model suitable for accident reconstruction were formulated. An instationary multipoint aerodynamics approach, based on blade element theory, met these demands. A "prescribed wake" model was then coupled with this multipoint aerodynamics approach to determine the induced velocities at all surfaces. The developed models were then validated and checked for plausibility with flight test data from a Schweizer SGS 1-36 sailplane.

For the purpose of describing the relations between pilot and aircraft behavior as well as launch safety, a flight envelope limiting airspeed and pitch attitude was proposed. It was shown that the aircraft's radius of gyration along its pitch axis influences the path taken through the flight envelope. As a consequence, motorglider conversions of existing sailplane designs operate closer to the upper pitch boundary of the flight envelope. With this knowledge a generic 18 m class motorglider model was then implemented in the developed aerodynamics model and exposed to a hypothetical accident scenario. Here it was shown that under the presented circumstances the risk of a pilot-provoked stall of the horizontal stabilizer exists. Depending on the severity of the stall, a catastrophic accident might result.

Foreword

The presented thesis is intended as my final project during my mechanical engineering studies at *RWTH Aachen University*. I was in the rather grateful position to continue my previous work in the research of winch launching as part of this thesis. Of course, the decision to dedicate this final thesis to sailplane research has been influenced by the very positive feedback and intense interest in the subject that the "Winch Launch Group" of the *Institute of Flight System Dynamics* has been confronted with in the past.

A number of persons have supported this project with their expertise and I am very much obliged to them. Dipl.-Ing. Martin Heide of *Alexander Schleicher GmbH & Co. Segelflugzeugbau* is the one who has come up with the initial idea of investigating winch launch accidents through the use of the *Institute's* winch launch simulation environment. He, as well as Dipl.-Ing. Michael Greiner, have been very supportive in providing insight into the design and development process of sailplanes. Particularly while visiting the *Schleicher* factory in Poppenhausen, Germany, their discussions proved to be particularly fruitful and sparked a handful of ideas.

Further thanks shall be expressed to Dipl.-Ing. Frank Stahlkopf and Frank Göldner of the *German Federal Bureau of Aircraft Accident Investigation* (*BFU*). Both gentlemen provided insight into the status of winch launch safety and accidents. It is also they who have enabled me to access the database of winch launch accidents registered by the *BFU*.

Two technically well-versed glider pilots have also contributed significantly to the project. Dipl.-Ing. Joachim Döring and Dipl.-Ing. Helge Mikuda gratefully shared their operational experience in flight operations and dedicated their personal time to support this research.

Dipl.-Ing. Andreas Gäb, my advisor, has been the one to be exposed to all the ups and downs of taking on such a project. From the onset he has been very supportive of the idea of expanding the winch launch simulation environment and has declared himself willing to tutor my work. His encouragement, particularly at times when progress was painstakingly slow, was irreplaceable.

Though Univ.-Prof. Dr.-Ing. Wolfgang Alles has by now retired from leading the *Institute of Flight System Dynamics* he still lent me valuable words of experience. Finally, thanks shall also be expressed to Univ.-Prof. Dr.-Ing. Dieter Moormann. As the *Institute's* new head, he continues to promote the research in the field of winch launching. It is he who provides the framework for continual work on the subject as an internal project.

The least I can do to recognize the aforementioned persons' contributions is to offer them a sincere "Thank You!"

Aachen, Germany,
in December of 2010

Christoph Santel

1 Statistical Analysis of Glider Winch Launch Accidents

Winch launching is the most widely used method for launching gliders throughout central and western Europe. In general, it is considered to be a safe and cost-effective means of providing a glider with adequate energy for free flight. However, every year, a number of accidents during the winch launch occur; a non-negligible number of which involve severe or fatal injury.

In order to receive a first quantitative understanding for the dangers involved in winch launching, it was decided to analyze historical data of accidents. For this purpose, the *German Federal Bureau of Aircraft Accident Investigation* ("Bundesstelle für Flugunfalluntersuchung", BFU) - located in Braunschweig, Germany - provided excerpts from its database of registered aircraft accidents [14]. The excerpts include all officially reported winch launch accidents that occurred within the territory of the Federal Republic of Germany, have involved German-registered gliders outside the territory of the Federal Republic of Germany, or in which the BFU has been asked to provide assistance in accordance with international treaties. The database excerpts span a time frame from 1983 to 2009 and include 477 entries of accidents which are suitable for analysis.

1.1 Methodology of Analysis

During analysis each accident is attributed to one of six possible phases of launch. These phases are proposed in accordance with a standardized questionnaire used by the BFU to register many of the accidents, as well as correlating them to the six phases of a regular, non-aborted, winch launch as is proposed by Apel [9]. In particular, these phases are:

- Before Ground Roll
- Ground Roll
- Initial Climb (until reaching the attitude necessary for main climb phase)
- Main Climb Phase (up to release altitude)
- Cable Release and Free Flight
- Aborted Launch

An illustration of a conventional launch trajectory and its corresponding phases is given in figure 1.1.

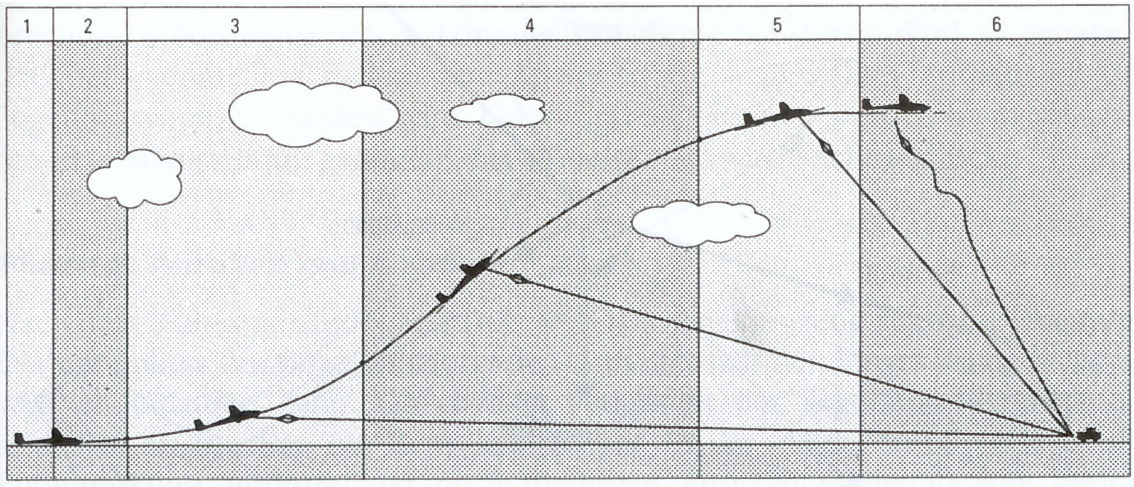

[Source: [9]]

Figure 1.1: Phases of the Winch Launch

The phase of winch launch, to which a given accident is attributed, is determined by identifying the point in time, during which the *initial* mistake or *primary* cause leading to the accident has occurred. Each accident is only attributed to one phase. Several examples of accidents attributed to a given phase of the winch launch are:

Before Ground Roll improperly hooked up control surfaces; multiple cables having been crossed unintentionally by ground personnel

Ground Roll wing tip touching ground or being restrained by high grass while the aircraft is still on ground

Initial Climb wing tip touching ground after the aircraft is airborne; aggressive behavior of the pilot to force the glider into a steep climb at low altitude

Main Climb Phase loss of control or stall once the glider has transitioned into quasi-steady climb

Cable Release and Free Flight loss of control after cable release; aircraft or other vehicles on ground being damaged by descending cable

Aborted Launch loss of power at the winch; hard landing as a result of intentionally practiced cable break procedures; loss of control after unintentional break of cable weak link

Additionally, for each phase of the winch launch, the number of accidents involving persons with fatal, severe or minor injury is counted. Also, the number of persons having received fatal, severe or minor injury is determined. The absolute number of accidents and persons involved in relation to the phases of winch launch is given in table 1.1. Some entries require further assumptions to be made in order to be categorized; such as estimating the altitude at which a loss of control occurred according the glider's impact attitude on the ground. A categorization of a small number of accidents is not possible since the database lacks an adequate description

of the events leading to these accidents. These uncategorized accidents are omitted in the ensuing analysis.

For each phase of flight, the relative number of accidents n_i is easily determined to

$$n_i = \frac{N_i}{\sum_i N_i}, \tag{1.1}$$

whereas N_i is the absolute number of accidents during launch phase i. The relative number of accidents answers to the question of *In which phase do most winch launch accidents happen?*

In their analysis, NEUHAUS ET AL. [25] inspect the safety record of general aviation accidents according to the category and class of aircraft involved. Hence, their work not only provides a structured methodology for inspecting such accidents statistically, but also contains reference values for the safety of glider operations. By staying within the definitions of the mentioned work, the probability of fatal injury $p_{f,i}$ in the course of an accident during launch phase i is defined as follows:

$$p_{f,i} = \frac{N_{f,i}}{N_i} \tag{1.2}$$

In this case $N_{f,i}$ defines the absolute number of accidents involving fatal injury during a given launch phase. The probability of severe injury $p_{s,i}$ and of minor injury $p_{m,i}$ during a given launch phase are defined analogously. These probabilities regard the question of *If an accident happens during a given launch phase, how likely is it that at least one person will be hurt/killed?* It shall be pointed out that the given definition of the probabilities of injury are conditional probabilities. Their significance is limited to the probability of receiving an injury in the case of an accident. They give no information about the general risk of injury during a given launch phase.

Accidents involving multiple degrees of injury will be accounted for in the multiple categories. If, for example, an accident involves a person with severe injury and another person with minor injury, it will be regarded in both $N_{f,i}$ and $N_{m,i}$. The BFU database does not explicitly register involved persons without injury. For these reasons it is only possible to estimate the minimum number of accidents without injury $N_{n,i,\min}$ in phase i.

$$N_{n,i,\min} = N_i - N_{f,i} - N_{s,i} - N_{m,i} \leq N_{n,i} \tag{1.3}$$

Hence, the minimum probability of sustaining no injury is defined as follows.

$$p_{n,i,\min} = \frac{N_{n,i,\min}}{N_i} \leq p_{n,i} \tag{1.4}$$

A further matter of interest is the question of *If an accident involving injury occurs during a given launch phase, how many people will be injured/killed?* This question is answered by the average number of persons killed $a_{f,i}$ during launch phase i. Its definition follows to

$$a_{f,i} = \frac{P_{f,i}}{N_{f,i}}. \tag{1.5}$$

Phase of Winch Launch	Symbol	Before Ground Roll	Ground Roll	Initial Climb	Main Climb Phase	Cable Release and Free Flight	Aborted Launch	$\sum$ of Winch Launches
# of Accidents - total	N_i	17	72	107	32	13	236	477
- involving fatal injury	$N_{f,i}$	1	2	25	9	2	14	53
- involving major injury	$N_{s,i}$	4	20	37	2	3	64	130
- involving minor injury	$N_{m,i}$	5	11	18	1	0	44	79
- involving no injury (est.)	$N_{n,i,\min}$	8	44	32	21	8	144	257
# of Persons - with fatal injury	$P_{f,i}$	1	2	25	9	2	16	55
- with major injury	$P_{s,i}$	4	20	37	2	3	73	139
- with minor injury	$P_{m,i}$	6	11	19	1	0	47	84

Table 1.1: Absolute Number of Accidents during Winch Launches of Gliders as Recorded by the BFU from 1983 to 2009

Here $P_{f,i}$ describes the number of persons fatally injured during launch phase i. Once again, the average number of persons receiving severe or minor injury, $a_{s,i}$ and $a_{m,i}$, are defined along the same lines.

The numeric values of the relative number of accidents, probabilities of injury and of the average number of persons involved is given in table 1.2, according to the respective phase of launch. For reasons of comparability, these values have also been determined for the winch launch in general as well as for all glider flights.

1.1.1 Analysis of Accident Data

When analyzing the data made available through the BFU database, it soon becomes apparent that we have to distinguish between accidents occurring as a result of an aborted launch and those initially taking place during a conventional launch phase. First, we shall study those accidents attributed to non-aborted launches. Here, we see that most accidents take place in the initial climb phase, soon followed by the ground roll phase. Accidents having their initial cause before the ground roll, during the main climb phase and during or after cable release are relatively rare and likely to end without injury. For all of these flight phases, the average number of persons involved in accidents rarely rises above one person. The significant rise of the average number of persons slightly injured during the ground roll with $a_{m,\text{Ground Roll}} = 1.20$ can be considered statistically insignificant due to the small number of accidents.

At the same time we see that the initial climb phase has the lowest minimum probability of sustaining no injury. This pays tribute to the fact that if an incident occurs in this phase of flight the pilot only has limited time and options available to cope with abnormal occurrences. Incidentally, injuries are more likely to occur.

Furthermore we shall take a more detailed look at the average numbers of persons killed or severely injured. According to Neuhaus et al. [25] these values are $a_{f,\text{Glider Flights}} = 1.13$ and $a_{s,\text{Glider Flights}} = 1.10$ for glider flights in general. We quickly see that for non-aborted winch launches, these numbers are significantly lower than for all glider flights. One possible conclusion to draw is that accidents are less likely to occur during non-aborted winch launches with a second person aboard. A possible explanation for this phenomenon is that the pilot is less likely to fly aggressively with a passenger aboard or that an instructor monitors the launch and intervenes appropriately before an accident occurs.

The highest risk of fatal injury during non-aborted launches occurs during the main climb phase, being almost three times as high as for the glider accidents in general[1]. It is soon followed by the risk of fatal injury in the initial climb. Yet the initial climb has the highest risk of severe injury, being over two times higher than that of all glider accidents. The ground roll soon follows the initial climb in regard to the risk of severe injury. One possible interpretation of these values is that as the potential and kinetic energies of the glider rise in the course of the launch, the risk and severity of the injuries received during an accident also rise. Hence, the risk of merely receiving slight injury is highest with accidents beginning before the ground roll. After cable release, the risk of fatal injury is reduced slightly and shifts back towards severe injury, accounting for the fact that the aircraft has sufficient altitude

[1] Keep in mind that these are conditional probabilities, requiring an accident to occur before a conclusion about the risk of injury can be drawn.

Phase of Winch Launch	Symbol	n_i	Before Ground Roll	Ground Roll	Initial Climb	Main Climb Phase	Cable Release and Free Flight	Aborted Launch	$\sum$ of Winch Launches	$\sum$ of Glider Flights[a]
Rel. # of Accidents			0.04	0.15	0.22	0.07	0.03	0.49	1.00	-
Probability of	- fatal injury	$p_{f,i}$	0.06	0.03	0.23	0.28	0.15	0.06	0.11	0.10
	- severe injury	$p_{s,i}$	0.24	0.28	0.35	0.06	0.23	0.27	0.27	0.15
	- minor injury	$p_{m,i}$	0.29	0.15	0.17	0.03	0.00	0.19	0.17	N/A
	- no injury (est.)	$p_{n,i,\min}$	0.47	0.61	0.30	0.66	0.62	0.61	0.54	N/A
Avg. # of Persons	- fatally injured	$a_{f,i}$	1.00	1.00	1.00	1.00	1.00	1.14	1.04	1.13
	- severely injured	$a_{s,i}$	1.00	1.00	1.00	1.00	1.00	1.14	1.07	1.10
	- slightly injured	$a_{m,i}$	1.20	1.00	1.06	1.00	-	1.07	1.06	N/A

Table 1.2: Statistic Values of Winch Launch Accidents According to Launch Phase

[a]Source [25]

for the pilot to react to an unforeseen situation with more options at hand.

Particular attention shall be heeded to aborted winch launches. We see that almost half of all winch launch accidents can be traced to an interruption in the launch sequence. At this point it shall be noted that launch interruptions might be unintentional or intentional. The case of a breaking weak link is usually unintentional; while intentional launch interruptions might be forced by an instructor releasing the tow cable at low altitude so that a student pilot can practice cable break procedures under supervision. These procedures are frequently practiced during primary flight training. While the risk of fatal injury is lower than average, the risk of severe injury is identical to the average risk of severe injury during winch launches. Particularly the average number of persons injured peaks in all three categories (fatal, severe and minor injury) during aborted launches. This hints to the fact that many accidents attributed to launch interruption are the result of intentional launch interruptions, since in this case an instructor is most often aboard. An all too common scenario is a hard landing or overshooting/undershooting a landing field while practicing cable break procedures. While landing accidents rarely end fatally, the risk of severe injury, particularly to the spine, is significant. It would appear that awareness to this risk should be accounted for in initial and recurrent training of glider flight instructors.

1.2 Conclusions with Regard to Ensuing Flight Dynamics Analysis

When disregarding the aborted launches, which often can be traced to mistakes while intentionally training cable break procedures, the initial launch phase is the most interesting. Here, the absolute numbers of accidents and persons injured is highest. It is also the most challenging to describe from a flight mechanics point of view. As the glider lifts off, it continues to accelerate further. It still lingers in ground effect while the rotation into a climbing attitude increases the load factor along the aircraft's vertical axis and therefore raises the glider's stall speed. As the glider rotates into the climb soon after lift-off, it exposes more of its ventral side to the winch. Therefore the component of the cable force acting on the glider increases along the glider's vertical axis. This serves to reduce the acceleration into the aircraft's vertical direction and leaves the pilot to perceive a lower than actual load factor[2] in this direction. The dynamics of the problem are aggravated further if the glider approaches a stall, as is the case during some loss-of-control-accidents which have occurred in the initial climb phase. An adequate flight mechanical description of these events would need to regard unsteady non-linear aerodynamics in ground effect. Yet the benefit of attempting to describe these accidents is an understanding of the mechanisms resulting in the highest numbers of injury during non-aborted launches.

[2]Recall that a pilot only feels the acceleration at the pilot's seat and not the angle of attack or load factors acting on the aircraft. In free flight, the translational acceleration of a glider is solely determined by the acting air and gravitational forces, their relation being described with load factors. During towed flight, the force of the tow cable exerted onto the glider also serves to contribute to the aircraft's motion.

2 Setup of Simulation

For the simulation of aircraft behavior during a winch launch accident, the winch launch simulation environment previously developed by the author [29] and his advising tutors [13] at the *Institute of Flight System Dynamics* is used. This control theory oriented flight simulation environment allows for interfacing of the major components and models interacting during the winch launch.

These components and models are

- the glider,
- the winch,
- the cable,
- the pilot and
- the winch operator.

A block diagram describing the interactions of these models is provided in figure 2.1.

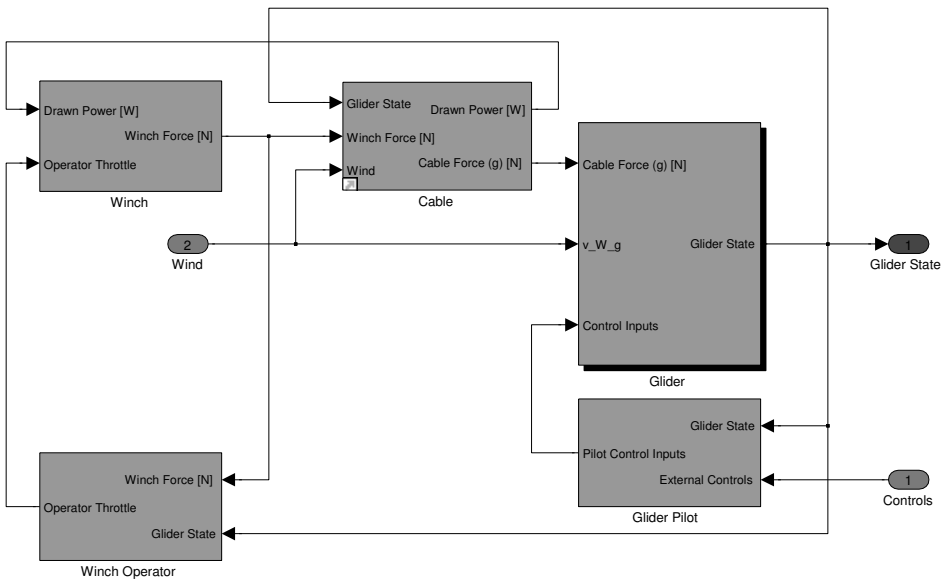

Figure 2.1: Block Diagram of the Winch Launch Simulation Environment

2.1 Aims of and Requirements to an Aerodynamics Model

Before starting an analysis of winch launch accidents it is necessary to clearly define the goals of the analysis. From these a series of demands for the necessary models needs to be derived. A way of meeting these demands then should be found.

The goal of this thesis is to gain a better understanding of the initial phases of the winch launch. Particularly the ground roll, lift-off and the transition into the climb are of interest. Furthermore, capabilities should be developed which allow for the study of accidents occurring within these phases. Gliders might be exposed to excessive pitch angles and angles of attack in proximity to the ground. During these phases they might also be prone to rolling inverted. It is a goal to depict these phenomena during analysis.

Having defined the aims of the research, it is now possible to deduce several demands. Translational and rotational accelerations during the initial phases of the winch launch can reach high values. Therefore their non-negligible influence on the instationary flight conditions needs to be captured. Furthermore, the phases to be studied occur in proximity to the ground, making an accurate depiction of the ground influence necessary. Also, the asymmetric aerodynamic conditions caused by high roll and yaw rates shall be duplicated. Finally, the flow conditions at all flight control surfaces shall be examinable in order to study their control margins, if necessary. All these demands are solely applicable to the aerodynamics model of the aircraft

It soon becomes evident that the single point aerodynamics approach utilized in previous studies by the author [29] and his advising tutors [13] is inadequate. Within this single point approach, all aerodynamic forces and moments are summarized onto reference point of the aircraft. They are only functions of the aircraft's freestream angles of attack and sideslip, the rotational rates and flight control deflections. This makes it extremely cumbersome to study the asymmetric flight mechanics conditions along the main wing or separately examine the tail surfaces. Ground effect influence is only modeled in a very rudimentary fashion, not depicting changes in the moment coefficients of the aircraft. At the same time, the parameters underlying the aerodynamics model were identified in stationary flight conditions, making the whole single point aerodynamics model quasi-stationary.

All these restrictions can be circumvented with a multipoint aerodynamics approach. Besides modeling all lifting surfaces separately and discretely, a wake model is necessary. By depicting the vortex sheets behind each lifting surface it is possible to study the effects of wingtip vortices as well as downwash at the stabilizers. This serves to couple the interactions of the different lifting surfaces through their induced velocities. Finally, the aerodynamic influence of the fuselage needs to be also included to allow for adequate prediction of flight performance.

2.2 Revised Aircraft Model

The aircraft is modeled as a rigid body allowed to move in six degrees of freedom (6DoF), with the Newtonian Equations of Motion describing the path of the air-

craft's center of gravity (CG). This implies that the aircraft's inertia is known in all available degrees of freedom. Within the simulation, the forces and moments caused by

- the ground,
- the airflow, and
- the tow cable

are determined and then used to calculate the aircraft's motion. All of these interfaces, with the exception of the aerodynamic modeling remain unchanged within the frame of the thesis.

2.2.1 Lifting Surfaces Modeling

As already mentioned, several flight conditions might occur during a winch launch accident which result in highly inhomogeneous flow conditions in the aircraft's spanwise direction. At the same time gliders are marked by a characteristically high aspect ratio. Similarly inhomogeneous flow conditions at high aspect ratios are found at the blades of helicopter rotors. A commonly used approach for grasping the aerodynamic effects of the flow around such rotor blades is the blade element theory (BET). It is presented in standard literature, such as by Bittner [10]. This theory, evaluated at multiple discrete points along a lifting surface's lifting line, is the basis for the multipoint aerodynamics approach applied in this thesis.

During the ensuing calculations the air is said to be an incompressible and inviscid fluid. This allows the flow field to be implicitly modeled as a potential flow field, which in turn enables standard aerodynamic formulas, namely Thomson's Theorem and the Biot-Savart Law, to be applied. Viscid parts of non-conservative aerodynamic forces, particularly the friction and pressure drag components, are also represented in the aerodynamics modeling by appropriately being regarded for each airfoil.

Geometric Considerations

Within BET the aircraft is modeled along its lifting surfaces. For a conventionally configured aircraft these are three surfaces; namely the wing, the horizontal tailplane and vertical tailplane. This approach treats each surface as being aerodynamically independent, with the only interaction being caused by each surface's wake acting on the other surfaces. Also, the aerodynamic effects of the fuselage are treated in a separate model.

Each lifting surface is identified by its index i_{surf} with the total number of lifting surfaces $n_{\text{surf}} = 3$ for a conventionally designed glider.

For each lifting surface, the lifting line is defined along $n_{ll} = n_{\text{pan}}(i_{\text{surf}}) + 1$ supporting points $\vec{r}_{ll}$. This creates a total of $n_{\text{pan}}(i_{\text{surf}})$ discrete panels along each lifting line. The index of each supporting point is i_{ll} and for each panel i_{pan}. Also, the type of lifting surface / primary function (e. g. main wing, stabilizer) and one airfoil per panel are attributed to each lifting surface. The following convention is applied to the enumeration of the supporting points of the lifting lines and panels:

On horizontally oriented lifting surfaces (e. g. main wing and horizontal stabilizer), the supporting points and panels are enumerated from port to starboard as seen in the direction of flight. The enumeration is from top to bottom for vertical surfaces (such as the vertical stabilizer).

Furthermore, for each panel the chord c_{pan} and the angle of incidence i has to be set.[1] All of these initially required geometric parameters are also gathered in table A.1.

From this rather limited amount of geometric data, a multitude of other geometric parameters can be easily determined, as seen in table A.2. This is done once, during the initialization of the simulation. These calculations are often trivial and therefore only a few of them are explained below.

The angles of panel sweep and dihedral are easily calculated with the coordinate transformations of appendix C. Here, the local y_p-axis is aligned with the lifting line on each panel. Also, it is assumed, that the aerodynamic panel center point[2] $\vec{r}_{\text{pcp}}$ is the geometric center point of the associated lifting line element.

The reference plane for determining the projected areas $S_{\text{proj}}(i_{\text{surf}})$ are the x_f-y_f-plane for all surfaces, except the vertical stabilizer. In this case the reference plane is the x_f-z_f-plane.

According to Thomas [33] the effectiveness of the vertical stabilizer is significantly increased in a T-tail configuration. This is attributed to the horizontal stabilizer acting as an end plate and reducing some of the aerodynamic losses associated with the three-dimensional flow around vertical stabilizer. Hence, he makes use of an effective aspect ratio $\Lambda_{\text{eff}} = 1.5\Lambda$ for the vertical stabilizer of a T-tail aircraft. For all other surfaces and configurations considered, the effective aspect ratio remains $\Lambda_{\text{eff}} = \Lambda$.

Reducing an actual aircraft to a geometric blade element model involves several steps. Figure 2.2 shall serve to illustrate this process. First, the location of the lifting lines of all aerodynamic surfaces must be defined. This is done by defining the location of lifting line support points $\vec{r}_{ll}$, which are marked by an "X" in the illustration. The distribution of the support points also serves to discretize the lifting line into panels. Now, further geometric properties and aerodynamic properties, such as chord, incidence and airfoil are attributed to each discrete panel. From this data, all other geometric parameters are derived as required and serve as the basis for all further aerodynamic calculations.

Local Airflow Conditions

The global aerodynamic conditions have been the basis for the formerly used single point aerodynamics approach. Here, only the relative translational and rotational motion between the aircraft's CG and the air are evaluated to allow for the prediction of the resulting aerodynamic forces and moments. Yet in the BET approach realized for this thesis, an evaluation of the aerodynamic conditions at every panel center point of every lifting surface becomes necessary.

The first aerodynamic calculation is the determination of the local vectorial

[1] For the definition of the angle of incidence, associated with the local panel-fixed coordinate system, refer to appendix C.

[2] This is the location on which all aerodynamic forces of a panel act upon.

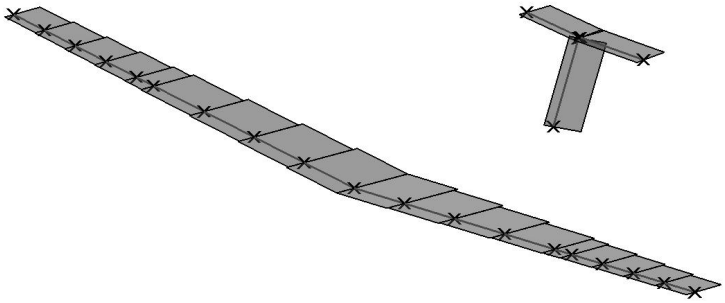

Figure 2.2: Geometric Blade Element Model of a Medium-Performance Sailplane

airspeed $\vec{V}_{A,\mathrm{loc},f}$ at each panel center point in aircraft body-fixed coordinates $_f$, as well as its corresponding scalar value $V_{A,\mathrm{loc}} = \left|\vec{V}_{A,\mathrm{loc},f}\right|$.

$$\vec{V}_{A,\mathrm{loc},f} = \vec{V}_{A,f} + \vec{\Omega}_{A,f} \times \vec{r}_{\mathrm{pcp},f} + \Delta\vec{V}_{A,\mathrm{ind},f} \tag{2.1}$$

Here $\vec{V}_{A,f}$ and $\Omega_{A,f}$ describe the aircraft CG's translational and rotational aerodynamic velocities in aircraft body-fixed coordinates. These are handed over into the aerodynamics calculation routine as solutions to the Newtonian Equations of Motion. Furthermore, $\Delta\vec{V}_{A,\mathrm{ind},f}$ is the contribution of induced velocities to the local airflow. This is discussed in more detail in the wake aerodynamics section of section 2.2.2.

Once again, all variables utilized in calculating the airflow are gathered in table A.3 and table A.4. Here it shall be noted that the local angles of attack and sideslip, α_{loc} and β_{loc} respectively, describe the local airflow in regard to the local panel-fixed coordinate system $_{p,\mathrm{loc}}$.

A graphic representation of the different local aerodynamic velocities is given in figure 2.3. The aircraft is simulated to initiate a right-hand turn, meaning that it has a positive roll rate $p_f > 0$. Several effects can be noted when studying the mentioned results. One sees that going from the left wingtip towards the right wingtip, the downward component of the local airspeed principally increases. This is due to the roll rate of the aircraft and can also be seen to have an effect on the horizontal tailplane. Particularly, on the left-hand wingtip, the downwash of the wingtip vortex is evident as the local angle of attack there is larger than on the adjacent panels.

Also, for determining the instationary aerodynamics coefficients in the ensuing section, the local geometric angle of attack $\alpha_{\mathrm{geo,loc}}$ is required. While for the conventional AOA, the total airspeed at the evaluation point is used, which consists of free airflow, rotational and induced components (see equation 2.1), this is not the case for the geometric AOA. It is solely calculated using the local geometric airspeed $\vec{V}_{A,\mathrm{geo,loc},f}$, which disregards the induced component.

$$\vec{V}_{A,\mathrm{geo,loc},f} = \vec{V}_{A,f} + \vec{\Omega}_{A,f} \times \vec{r}_{\mathrm{pcp},f} \tag{2.2}$$

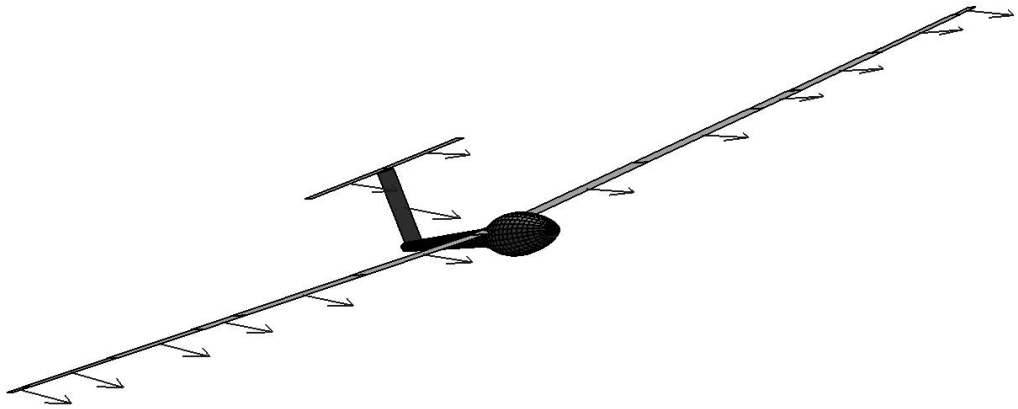

Figure 2.3: Local Aerodynamic Velocities $\vec{V}_{A,\mathrm{loc}}$ on a High-Performance Sailplane Initiating a Right-Hand Turn

The reason for this formulation is to avoid numeric instabilities in the wake. Such instabilities can be excited by the coupling of wake intensity and induced velocities at each panel.

For determining the local Reynolds Number $Re_{\mathrm{loc}} = \frac{\rho}{\mu} \cdot V_{A,\mathrm{loc}} \cdot c_{\mathrm{pan}}$, knowledge of the local air density ρ and dynamic viscosity μ becomes necessary. Both of these values are gathered from the International Standard Atmosphere (ISA), as provided by RUIJGROK [28]. This lookup is performed by evaluating the function `ISA_Ruijgrok.m` at the present aircraft CG's altitude and therefore disregarding variations of ISA values along the aircraft's geometry.

Local Aerodynamic Forces and Moments

For the time being, each panel is considered to provide lift, drag and an aerodynamic pitching moment. At each panel a local aerodynamic coordinate system (index $_{a,\mathrm{loc}}$) and panel-fixed coordinate system (index $_{p,\mathrm{loc}}$) are defined. Hence, the flow around each element only creates lift in the direction of the local $z_{a,\mathrm{loc}}$-axis and drag in the direction of the local $x_{a,\mathrm{loc}}$-axis. The aerodynamic moment is assumed to act perpendicular to the airfoil, along the $y_{p,\mathrm{loc}}$-axis, rather than perpendicular to the local lift and drag. Also,the magnitude of all aerodynamic forces and moments is only influenced by the component of the airflow normal to the lifting line of each panel. This is in accordance with VAN DER WALL's lectures [35] on blade element theory.

Yet the question arises of how to predict the local contributions to lift, drag and aerodynamic moment. The primary influence on these parameters is expected to be the type of airfoil utilized. Also, it is assumed, that only angle of attack α, Reynolds Number Re and flap deflection angle δ influence the stationary lift, drag and moment coefficients $C_{l,\mathrm{stat}}$, $C_{d,\mathrm{stat}}$ and $C_{m,\mathrm{stat}}$ of a given airfoil in stationary flow. The interdependencies

$$C_{l,\mathrm{stat}} = C_{l,\mathrm{stat}}(\alpha, Re, \delta) \tag{2.3a}$$

$$C_{d,\mathrm{stat}} = C_{d,\mathrm{stat}}(\alpha, Re, \delta) \tag{2.3b}$$

$$C_{m,\mathrm{stat}} = C_{m,\mathrm{stat}}(\alpha, Re, \delta) \tag{2.3c}$$

of all airfoils utilized in an aircraft model analyzed are required as input in form of lookup tables into the simulation.

Of course, the assumption of stationary airflow during the winch launch accidents appears to be unsustainable. As previously mentioned, such accidents are characterized by highly dynamic maneuvers. JOHNSON [19] provides a simple model for predicting the dynamic influences of the of angle of attack variations on the lift and moment coefficients of an airfoil. The dynamic coefficients are solely functions of the static coefficients as well as the temporal derivative of the geometric angle of attack in non-dimensional form[3] $\dot{\alpha}^{\star}_{\text{geo}} = \dot{\alpha} \cdot \frac{c}{V_{A,\text{geo}}}$. This allows for a simplified regard of dynamic effects such as lift-coefficient overshoot at highly dynamic changes in angle of attack and dynamic lift hysteresis.

$$C_{l,\text{dyn}} = \begin{cases} C_{l,\text{stat}} + (3 - C_{l,\text{stat}}) \cdot 20\dot{\alpha}^{\star}_{\text{geo}} & \dot{\alpha}^{\star}_{\text{geo}} < 0.05 \\ 3 & \dot{\alpha}^{\star}_{\text{geo}} \geq 0.05 \end{cases} \tag{2.4a}$$

$$C_{d,\text{dyn}} = C_{d,\text{stat}} \tag{2.4b}$$

$$C_{m,\text{dyn}} = \begin{cases} C_{m,\text{stat}} & \dot{\alpha}^{\star}_{\text{geo}} < 0.02 \\ C_{m,\text{stat}} - & \\ (0.8 + C_{m,\text{stat}}) \cdot \left(33.3\dot{\alpha}^{\star}_{\text{geo}} - 0.667\right) & 0.02 \leq \dot{\alpha}^{\star}_{\text{geo}} < 0.05 \\ -0.8 & \dot{\alpha}^{\star}_{\text{geo}} \geq 0.05 \end{cases} \tag{2.4c}$$

One should note that JOHNSON's formulations do not regard boundaries for negative changes in AOA; $\dot{\alpha}^{\star}_{\text{geo}} < 0$.

Though this model has been postulated and validated for helicopter airfoils, it is assumed that the results are also usable for the laminar flow airfoils often found in gliders. Furthermore, several words about the determination of $\dot{\alpha}^{\star}_{loc}$ are in order. While not explicitly mentioned by JOHNSON [19], it is deemed most likely that the temporal derivative of the geometric AOA is the basis for transfer of stationary to dynamic coefficients. During the associated wind tunnel experimentation in which the corresponding two-dimensional airfoil data is measured, often only temporal changes in the experimental pitch angle of the airfoil are available. Without the induced velocities being available for the analysis of the experiments, it seems plausible that JOHNSON's model is based on the geometric AOA.

In JOHNSON's model $\dot{\alpha}^{\star}_{geo,loc}$ contains a component contributed by translational ("upward/downward") acceleration of the wing panel, which in turn might be caused by a rolling acceleration of the aircraft. LEISHMAN [22] discusses that the reformulation of the translational acceleration (lead-lag and flapping motions for helicopter rotor blades) of an airfoil as a change in $\dot{\alpha}^{\star}$ (a change in airfoil pitch speed during wind tunnel testing), will cause some error in the results achieved. Yet this methodology is often agreed upon within the helicopter aerodynamics community, as it reduces the number of independent parameters during experimentation and calculation.

It is assumed that each panel's lift, drag and moment coefficients - $C_{L'}$, $C_{D'}$ and $C_{M'}$ respectively - are identical to the two-dimensional dynamic coefficients of the airfoil of each panel.

[3] This form is somewhat atypical, since in other literature $\dot{\alpha}^{\star}$ is often found to be $\dot{\alpha}^{\star} = \frac{c}{2V_A}$.

$$C_{L'} = C_{l,\mathrm{dyn}} \tag{2.5a}$$
$$C_{D'} = C_{d,\mathrm{dyn}} \tag{2.5b}$$
$$C_{M'} = C_{m,\mathrm{dyn}} \tag{2.5c}$$

The corresponding panel lift L', panel drag D' and panel moment M' are determined by the means of standard blade element theory, according to VAN DER WALL [35].

$$L' = \frac{\rho}{2} \cdot V_{A,\mathrm{loc}}^2 \cdot \cos^2 \beta_{\mathrm{loc}} \cdot S_{\mathrm{pan}} \cdot C_{L'} \tag{2.6a}$$
$$D' = \frac{\rho}{2} \cdot V_{A,\mathrm{loc}}^2 \cdot \cos^2 \beta_{\mathrm{loc}} \cdot S_{\mathrm{pan}} \cdot C_{D'} \tag{2.6b}$$
$$M' = \frac{\rho}{2} \cdot V_{A,\mathrm{loc}}^2 \cdot \cos^2 \beta_{\mathrm{loc}} \cdot S_{\mathrm{pan}} \cdot c_{\mathrm{pan}} \cdot C_{M'} \tag{2.6c}$$

For the detailed prediction of the wake of each lifting surface, the circulation Γ_{pan} of each panel must also be determined. This is done under the assumption of a constant circulation along the width b_{pan} of the lifting line of each panel. KOTHMANN ET AL. [21] suggest on the basis of the instationary BERNOULLI'S principle that lift and circulation do not correspond instantaneously. Changes in panel circulation Γ_{pan} much rather lag behind changes in panel lift L'.

$$\Gamma_{\mathrm{pan}} = \frac{L'}{b_{\mathrm{pan}} \cdot \rho \cdot V_{a,\mathrm{loc}}} - k_{\mathrm{circ}} \cdot \frac{c_{\mathrm{pan}}}{2V_{A,\mathrm{loc}}} \dot{\Gamma}_{\mathrm{pan}} \tag{2.7}$$

In an attempt to positively influence the numeric stability of the wake, a correction factor k_{circ} is introduced in this thesis to further modify the delay behavior. Typical values selected for k_{circ} vary in the interval of $0 \leq k_{\mathrm{circ}} \leq 1$.

Now that the magnitude and orientation of all aerodynamic forces and moments of each panel are known, the aerodynamic contribution of each panel on the forces and moments acting on the aircraft's CG is formulated in aircraft body-fixed coordinates. Staying within our conventions, $\vec{F}_{A,\mathrm{loc},f}$ describes the corresponding force and $\vec{M}_{A,\mathrm{loc},f}$ the corresponding moment.

$$\vec{F}_{A,\mathrm{loc},f} = -\boldsymbol{M}_{fp} \cdot \boldsymbol{M}_{pa,\mathrm{loc}} \cdot \begin{pmatrix} D' \\ 0 \\ L' \end{pmatrix}_{A,\mathrm{loc}} \tag{2.8a}$$
$$\vec{M}_{A,\mathrm{loc},f} = \boldsymbol{M}_{fp} \cdot \begin{pmatrix} 0 \\ M' \\ 0 \end{pmatrix}_{p} + \vec{r}_{\mathrm{pcp},f} \times \vec{F}_{A,\mathrm{loc},f} \tag{2.8b}$$

The formulation that the local aerodynamic moment M' of each panel is oriented along the local y_p-axis underlies some further restrictions. Within this formulation, the orientation[4] is independent of the local angle of sidelip β_{loc}. LEISHMAN [22]

[4] though not the magnitude

indicates that this assumption is generally valid for attached airflow. As soon as airflow begins to separate the orientation begins to change, with β_{loc} significantly contributing to this reorientation.

As a final step, the calculation of the aerodynamic forces $\vec{F}_{A,ls,f}$ and moments $\vec{M}_{A,ls,f}$ created by all lifting surfaces at once is a simple summation.

$$\vec{F}_{A,ls,f} = \sum_{i_{\text{surf}}=1}^{n_{\text{surf}}} \sum_{i_{\text{pan}}=1}^{n_{\text{pan}}} \vec{F}_{A,\text{loc},f}\left(i_{\text{surf}}, i_{\text{pan}}\right) \tag{2.9a}$$

$$\vec{M}_{A,ls,f} = \sum_{i_{\text{surf}}=1}^{n_{\text{surf}}} \sum_{i_{\text{pan}}=1}^{n_{\text{pan}}} \vec{M}_{A,\text{loc},f}\left(i_{\text{surf}}, i_{\text{pan}}\right) \tag{2.9b}$$

Those available parameters associated with the local and total aerodynamic forces and moments are also documented in table A.5.

2.2.2 Wake Model

In order to be able to predict the local angles of attack α_{loc} at each panel, detailed knowledge of the local induced velocities $\Delta\vec{V}_{A,\text{ind}}$ is necessary. For this reason a "prescribed" or "trailed" wake model is implemented for each lifting surface. While a "free wake" model allows for a detailed study of the vortices, and allows the modeling of phenomena such as vortex roll up in the far field, it does so at a significant numerical cost and complexity. Hence, the selected "trailed wake" does not change its geometry due to self induction. It is assumed that it is solely trailed downstream of each lifting surface by the free-stream aerodynamic translational and rotational velocities of the aircraft $\vec{V}_A$ and $\vec{\Omega}_A$. This allows for the wake to be displaced according to the aircraft's maneuvering, a modeling feature not available in the less complex "rigid wake" models where the wake is geometrically fixed to each lifting surface.

Wake Geometry

The conventional lifting line theory of PRANDTL, which is treated in standard texts such as by SCHLICHTING and TRUCKENBRODT [30], assumes that a vortex sheet is created by each lifting surface and trailed downstream. For the purpose of this model, this vortex sheet is discretized into a finite number of vortices being either oriented parallel to the direction of the free airflow – so called trailed vortices – or parallel to the lifting line element's local y_p-axis – so called shed vortices – at the instant of vortex creation.

A total of $n_{tr} = n_{\text{pan}} + 1$ discrete trailing vortices exist for each lifting surface and are streamed from each support point of the corresponding lifting line. The enumeration of each trailing vortex i_{tr} follows the same convention as the enumeration of each panel, with the port-most / upper-most trailing vortex receiving the lowest index $i_{tr} = 1$ and the starboard-most / lower-most trailing vortex being identified as $i_{tr} = n_{tr}$. Each trailing vortex is then divided into a total of $n_{tr,\text{sec}} = n_{sh} - 1$ straight-line vortex sections with the intensity $\Delta\Gamma_{tr}(i_{tr}, i_{tr,\text{sec}})$. Here n_{sh} indicates the total number of discrete shed vortices of the appropriate lifting surface.

While the vortex sheet in flight will be of an infinite length, this is not easily compatible with the numeric formulation of the problem at hand. Instead, a total of n_{sh} discrete vortices is regarded, with all other shed vortices and trailing vortex sections flowing past the n_{sh} vortex's position being truncated from the problem. These shed vortices are also divided into a total of $n_{sh,\mathrm{sec}} = n_{tr} - 1$ straight-line vortex sections with the intensity $\Delta\Gamma_{sh}(i_{sh}, i_{sh,\mathrm{sec}})$. Here, the convention applies that during all time-step iterations, the shed vortex coinciding with the lifting line receives the index $i_{sh} = 1$ while the shed vortex being farthest downstream receives the index $i_{sh} = n_{sh}$.

n_{sh} is determined by the demand that at a given reference airspeed V_{ref}, the downstream wake length in stationary flight shall extend at least a multiple of k_{span} wingspans downstream.

$$n_{sh} = 1 + \left\lceil \frac{k_{\mathrm{span}} \cdot b_{\mathrm{proj}}}{V_{\mathrm{ref}} \cdot \Delta t} \right\rceil \tag{2.10}$$

The described vortex geometry implies that each shed vortex intersects with every trailing vortex and vice versa. Therefore, a "net" of $n_{sh} \cdot n_{tr}$ wake support points $\vec{r}_{\mathrm{wsp}}$ exist, with one being located at each intersection. The shed vortex index of each wake support point also increases by a value of one for each time-step, due to the wake support points moving downstream.

$$\vec{r}_{\mathrm{wsp},f}\left(i_{sh}, i_{tr}\right)\big|_t = \begin{cases} \vec{r}_{ll,f}\left(i_{tr}\right) & i_{sh} = 1 \\ \overbrace{\vec{r}_{\mathrm{wsp},f}\left(i_{sh}-1, i_{tr}\right)\big|_{t-\Delta t}}^{\text{previous position}} - \overbrace{\vec{V}_{A,f} \cdot \Delta t}^{\text{translational drift}} & \\ \quad - \underbrace{\vec{\Omega}_{A,f} \times \vec{r}_{\mathrm{wsp},f}\left(i_{sh}-1, i_{tr}\right)\big|_{t-\Delta t} \cdot \Delta t}_{\text{rotational drift}} & 2 \le i_{sh} \le n_{sh} \end{cases} \tag{2.11}$$

The geometry of the explicit trailed wake model of an medium-performance glider undergoing a stationary maneuver is sketched in figure 2.4. Each wake support point $\vec{r}_{\mathrm{wsp}}$ is clearly marked.

Wake Intensity

As already mentioned, two different types of vortices compose the wake of each lifting surface; trailing vortices and shed vortices. Considering that the trailing vortex intensity is only a function of the circulation distribution of the main wing at the instant of vortex creation, it can be interpreted as the stationary component of the solution to the lifting line theory. Anderson et al. [8] [7] provide a discrete model for numerical calculations of a single surface with arbitrary airfoils, much similar to the model derived above. Though in contrast to the Anderson model, the semi-infinite straight-line trailing vortex elements have been replaced by the truncated trailing vortices of the "prescribed" geometry. Also, Anderson et al. only regard one single lifting surface out of ground effect.

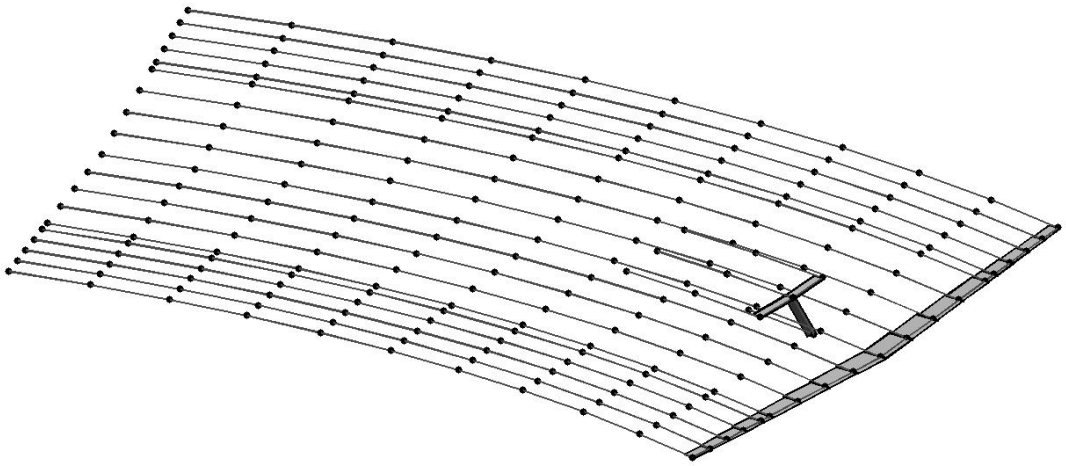

Figure 2.4: Trailed Wake of a Medium-Performance Glider during Stationary Maneuvering

The first vortex element of each trailed vortex averages the influence of the lifting surface's circulation distribution between the previous and current time-step.[5] Its intensity is determined by the derivative of the circulation along the lifting line $\frac{\partial \Gamma_{\text{pan}}}{\partial y_p}$. Analogous to ANDERSON ET AL., the following discrete formulation of the trailing vortex intensity $\Delta\Gamma_{tr}$ is selected.

$$\Delta\Gamma_{tr}\left(i_{tr}, i_{tr,\text{sec}}\right)\big|_t = \begin{cases} -k_{\text{tip}}\Gamma_{\text{pan}}\left(i_{tr}\right) & i_{tr}=1, i_{tr,\text{sec}}=1 \\ -\left[\Gamma_{\text{pan}}\left(i_{tr}\right)-\Gamma_{\text{pan}}\left(i_{tr}-1\right)\right] & \begin{array}{l}2\le i_{tr}\le n_{tr}-1\\ i_{tr,\text{sec}}=1\end{array} \\ k_{\text{tip}}\Gamma_{\text{pan}}\left(i_{tr}-1\right) & i_{tr}=n_{tr}, i_{tr,\text{sec}}=1 \\ \Delta\Gamma_{tr}\left(i_{tr}, i_{tr,\text{sec}}-1\right)\big|_{t-\Delta t} & 2\le i_{tr,\text{sec}}\le n_{tr,\text{sec}} \end{cases} \tag{2.12}$$

As can be seen, only the first vortex sections $i_{tr,\text{sec}} = 1$ are influenced by the lifting surface's circulation distribution. These are then convected to the next downstream elements.

Particular care needs to be given to the formulation of the trailing vortices at the tips of each lifting surface. At the tip, a zero-circulation / zero-lift boundary condition exists. This - along with the fact that during most expected flight conditions the function $\Gamma_{\text{pan}}\left(y_p\right)$ will have a right-hand curvature with $\frac{\partial^2 \Gamma_{\text{pan}}}{\partial y_p^2} < 0$ - serves to underestimate tip vortex intensity, if a conventional finite differences formulation of $\frac{\partial \Gamma_{\text{pan}}}{\partial y_p}$ is used. In order to alleviate some of the errors made in this approach, the tip correction factor k_{tip} is introduced.

For the case of a steady circulation distribution ANDERSON ET AL. [8] validate their model. Apparently, results are particularly favorable with angles of attack

[5] The center points of the first trailing vortex elements already have convected downstream slightly. It is the midpoint between the lifting line and second shed vortex elements.

ranging close to stall. However, for stalled wing panels, the description of the airflow cannot be interpreted as being precise in any way, though a first-order "engineering estimate" of forces and moments can still be reached. The model derived within this thesis is expected to provide similar results for the main wing in steady state flight out of ground effect. This is due to the very similar wake structure, with the truncated wake sections not contributing to the downwash at the wing in a significant manner. Also, the effects of lifting surface interaction - which will be described in the ensuing passages - is negligible for the influence of the tail surfaces acting on the main wing. The inverse cannot be said for the influence of the main wing acting onto the tail surfaces.

If the trailing vortices are interpreted as being the stationary part of the wake solution, then the shed vortices are the instationary part. A prominent example of a shed vortex is the starting vortex of an aircraft beginning its take-off ground roll. Shed vortices are a function of the derivative $\frac{\partial \Gamma_{\text{pan}}}{\partial t}$. The problem of discrete formulation of the shed vortex circulation $\Delta\Gamma_{sh}$ already has been tackled by PISZKIN and LEVINSKY [26]. Yet it has been found that this explicit formulation of the shed vortices has a detrimental effect on numeric stability of the lifting surface / wake interaction.

For this reason, and due to the high numeric cost associated with evaluating the high number of shed vortices in the prescribed wake, it has been decided to only evaluate the bound vortex of the lifting line of each lifting surface. By implying that the shed vortex flows downstream and only affects the lifting surface which created any given shed vortex, it is possible to formulate changes in panel circulation Γ_{pan} as having a first order delay to changes in panel lift L'. Equation 2.7 is the mathematical formulation of this relationship.

According to JOHNSON [20], the assumption that the shed vortex only acts onto the lifting surface creating it and therefore acts as a first-order delay between blade element lift and circulation is also present in the *ONERA EDLIN* rotorcraft aerodynamics code. The assumption that a shed wake does not affect the other lifting surfaces is also implied by JATEGAONKAR and GOPALRATNAM [16]. Their model couples the downwash acting on the horizontal stabilizer of an aircraft to main wing lift by introducing a fixed reaction time delay between the two. This reaction time is a direct function of the freestream velocity and the distance between main wing and stabilizer. The downstream convection of trailed vortices from the main wing, with the panel circulation lagging behind changes in lift by a first order differential equation, can be seen as a explicit formulation of the assumptions made by JATEGAONKAR and GOPALRATNAM [16] for wing / stabilizer interaction.

Wake-Induced Velocities

Now that the full geometry of each wake is known - along with its intensity - it is easily possible to calculate the induced velocity $\Delta V_{A,\text{ind}}$ at an arbitrary evaluation point $\vec{r}_{\text{eval}}$.

Determining the magnitude ΔV_{vort} of the velocity induced by a straight line vortex section of the intensity Γ at an arbitrary evaluation point $\vec{r}_{\text{eval}}$ is a standard and planar problem of fluid dynamics.[6] Its analytical solution is given in standard

[6] for the case that no ground effect is present

texts, such as by TRUCKENBRODT [34]. The geometry of the problem is provided in figure 2.5.

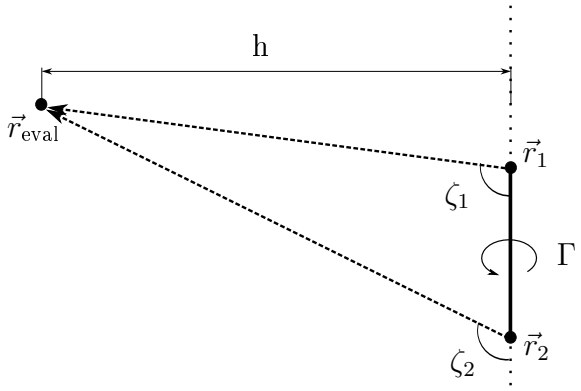

Figure 2.5: Geometry of Straight-Line Vortex Element Inducing a Velocity an Evaluation Point $\vec{r}_{\text{eval}}$

The corresponding wake support points $\vec{r}_{wsp}$ will act as beginning and end points $\vec{r}_1$ and $\vec{r}_2$ for the vortex element. Accordingly, the opening angles ζ_1 and ζ_2 are defined as

$$\zeta_1 = \angle\left(\vec{r}_{\text{eval}} - \vec{r}_1\right), \left(\vec{r}_2 - \vec{r}_1\right) \tag{2.13a}$$

$$\zeta_2 = \angle\left(\vec{r}_{\text{eval}} - \vec{r}_2\right), \left(\vec{r}_2 - \vec{r}_1\right) \tag{2.13b}$$

h describes the normal distance between the vortex axis and the evaluation point $\vec{r}_{\text{eval}}$. Utilizing the solution of TRUCKENBRODT [34], the induced velocity of the vortex is determined to

$$\Delta V_{\text{vort}} = \begin{cases} 0 & h < h_{\min} \vee h > h_{\max} \\ \\ \frac{\Gamma}{4\pi}\frac{\cos\zeta_1 - \cos\zeta_2}{h} & h_{\min} \leq h \leq h_{\max} \end{cases} \tag{2.14}$$

In order to prevent the divergence of the solutions for evaluations close to the vortex element, the velocity is set to zero if h drops beneath a predefined critical value $h_{\min}$. Also, for large distances $h > h_{\max}$ the velocity is also set to zero to prevent the solutions from dropping below the computer's machine accuracy.

Finding the orientation of the vector $\Delta\vec{V}_{\text{vort}}$ is a simple exercise, with the direction being determined by

$$\frac{\Delta\vec{V}_{\text{vort}}}{\Delta V_{\text{vort}}} = \begin{cases} \frac{(\vec{r}_{\text{eval}} - \vec{r}_1) \times (\vec{r}_2 - \vec{r}_1)}{|(\vec{r}_{\text{eval}} - \vec{r}_1) \times (\vec{r}_2 - \vec{r}_1)|} & h \geq h_{\min} \\ \\ 0 & h < h_{\min} \vee h > h_{\max} \end{cases} \tag{2.15}$$

The mentioned steps of determining $\Delta\vec{V}_{\text{vort}}$ for a series of evaluation points is implemented in the function `DeltaV_of_Vortex.m`.

One has to keep in mind that the induced velocity mentioned above does not regard any ground effect. In order to allow for the inclusion of the ground effect, which particularly influences the downwash velocities induced by the wake, an "image" or "mirror plane" approach is selected. For illustrative purposes, a graphical

representation of this method is given in figure 2.6. Here, each vortex filament is mirrored on a mirror plane parallel to the x_g-y_g-axis at an elevation of $z_{mp,g}$. The component of the induced velocity attributed to ground effect is $\Delta\vec{V}_{\text{vort},ge}$. More precisely, this approach includes the following steps:

1. mirror $\vec{r}_{\text{eval}}$ on mirror plane to receive $\tilde{\vec{r}}_{\text{eval}}$
2. calculate $\Delta\tilde{\vec{V}}_{\text{vort},ge} = \Delta\vec{V}_{\text{vort}}\left(\tilde{\vec{r}}_{\text{eval}}\right)$
3. mirror $\Delta\tilde{\vec{V}}_{\text{vort},ge}$ on mirror plane to receive $\Delta\vec{V}_{\text{vort},ge}$

The total velocity induced by a single straight-line vortex section is now easily determined to be $\vec{V}_{\text{vort}} = \Delta\vec{V}_{\text{vort}} + \Delta\vec{V}_{\text{vort},ge}$.

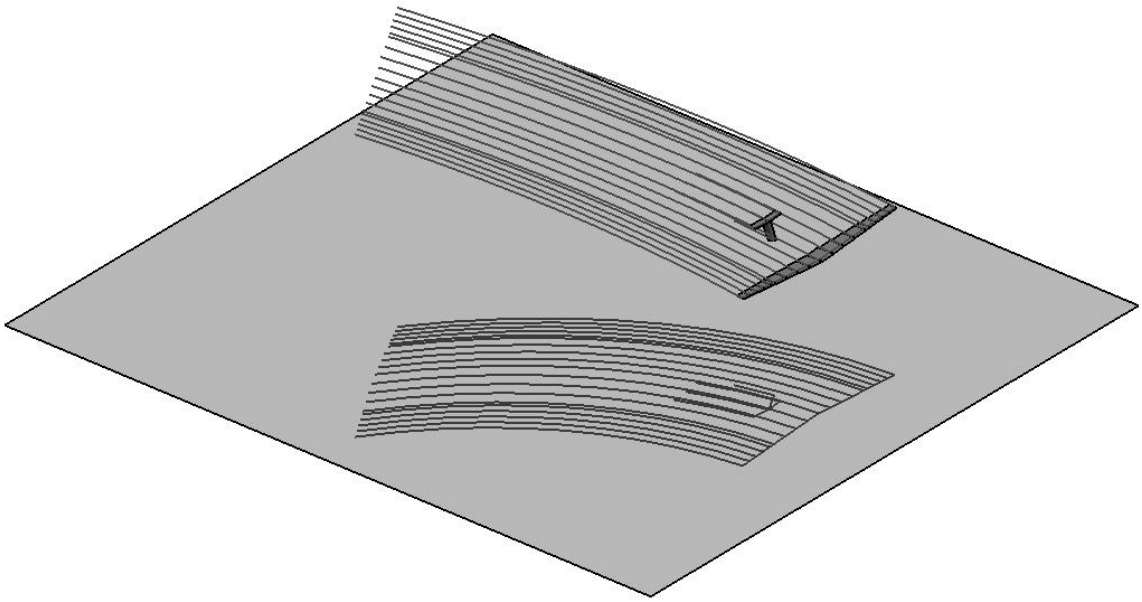

Figure 2.6: Trailed Wake Vortices Reflected on a Mirror Plane

The total induced velocity ΔV_{wake} created by all wakes in ground effect is determined by superposing corresponding velocities of every single vortex section.[7]

$$\Delta\vec{V}_{\text{wake}} = \sum_{i_{\text{wake}}=1}^{n_{\text{wake}}} \left(\sum_{i_{\text{pan}}=1}^{n_{\text{pan}}} \vec{V}_{\text{vort,ge}} + \sum_{i_{tr}=1}^{n_{tr}} \sum_{i_{tr,\text{sec}}=1}^{n_{tr,\text{sec}}} \vec{V}_{\text{vort,ge}} \right) \tag{2.16}$$

This velocity is the actual motion of the air, as it is caused by the wake. In order to be able to superimpose this onto the free airflow and utilize for the determination of the aerodynamic conditions at each panel, the orientation is changed into the opposite direction.

$$\Delta\vec{V}_{A,\text{ind}} = -\Delta\vec{V}_{\text{wake}} \tag{2.17}$$

[7] Recall that only the trailing vortices as well as the bound vortices of each lifting surface are explicitly modeled.

By evaluating $\Delta\vec{V}_{A,\text{ind}}$ at each panel of each lifting surface, a task performed by the `DeltaV_at_panels.m`-function, the loop back to section 2.2.1 is completed. Here, the wake-induced velocities influence the aerodynamic conditions at each panel, which in turn, contribute to the local circulation at each panel. This once again propagates into the wake intensity for shed and trailed vortices, which again influence the wake-induced airspeeds. For simplified reference those wake variables accessible for analysis are also given in table A.6.

2.2.3 Initialization of Wake

While the winch launch simulation environment usually starts with the aircraft being at a standstill, this by no means implies that the glider experiences no airspeed. Particularly, when wind is present, the non-moving aircraft will already have a developed wake, which for the case of initialization is considered to be stationary. The geometry of this stationary wake is easily calculated by assuming constant translational and rotational airspeeds at the moment of initialization. This task is performed by the `initialization_of_wake.m` function. It returns the location of all wake support points $\vec{r}_{wsp,f}\,(i_{sh}, i_{tr})$ and retains all trailing vortex circulation intensities at $\Delta\Gamma_{tr} = 0$.

Yet particularly, a fully developed circulation distribution along each lifting surface is required for the simulation to run in a stable fashion. This circulation distribution is then coupled with the wake of each surface according to the laws presented in section 2.2.2. This initialization of the panel circulation distribution and wake intensity is performed in the `circulation_converger.m` function and is structured much similar to the circulation convergence algorithm of Anderson et al. [8].

The previously mentioned MATLAB function particularly performs the following steps. Corresponding variables which need to be predefined are found in table A.7.

1. Determine the circulation $\Gamma_{\text{pan,new}}$ of each panel of every lifting surface using the `converger_aerodynamics.m` function.

2. Set all panel circulations to $\Gamma_{\text{pan}} = \Gamma_{\text{pan,old}} + D_{\text{conv}}\,(\Gamma_{\text{pan,new}} - \Gamma_{\text{pan,old}})$. Here D_{conv} is a constant to dampen convergence.

3. Calculate the intensity of each trailed vortex and set the intensity constant along the total vortex length (steady state initialization).

4. Determine the convergence parameter ε.

$$\varepsilon = \frac{1}{n_{\text{surf}}} \sum_{i_{\text{surf}}=1}^{n_{\text{surf}}} \frac{\sqrt{\sum_{i_{\text{pan}}=1}^{n_{\text{pan}}} \left(\frac{\Gamma_{\text{pan,new}} - \Gamma_{\text{pan,old}}}{\Gamma_{\text{pan,new}}}\right)^2}}{n_{\text{pan}}} \tag{2.18}$$

5. Set $\Gamma_{\text{pan,old}} = \Gamma_{\text{pan,new}}$.

6. Repeat steps 1 through 5 until $\varepsilon \leq \varepsilon_{\max}$ or the maximum number of iterations $n_{\text{iter,max}}$ is reached.

7. If the maximum number of iterations is reached while $\varepsilon > \varepsilon_{\max}$, then the solution is considered to remain unconverged and the simulation is aborted.

2.2.4 Aerodynamic Effects of the Fuselage

Aside from the lifting surfaces, whose modeling has been thoroughly discussed in the preceding sections, it is also necessary to include an aerodynamics model of the fuselage to receive adequate results. The fuselage is proposed to be a slender body of rotational symmetry, such as studied by ALTHAUS [5]. It is further considered to be solely exposed to the free airflow.

From a force perspective, the inner panels of the main wing protrude into the fuselage geometry. Therefore, only fuselage drag D_{fu} is modeled within this thesis, with any fuselage lift being accounted for by the inner wing panels. Moment effects of the fuselage are also disregarded. Neither has a ground effect model been incorporated into the corresponding `fuselage_aerodynamics.m` function. The same assumption of disregarding fuselage lift is also made in the glider design text of ZAMYATIN [36].

In the studies of ALTHAUS [5], the fuselage drag coefficient $C_{D,fu}$ is identified as a function of the fuselage Reynolds Number $Re_{fu} = \frac{\rho}{\mu} \cdot V_A \cdot l_{fu}$ as well as the fuselage angle of attack α_{fu}.

$$C_{D,fu} = C_{D,fu}\left(\alpha_{fu}, Re_{fu}\right) \tag{2.19}$$

Here, $V_a = \left|\vec{V}_a\right|$ is the magnitude of the free stream velocity and l_{fu} is the length of the fuselage along its axis of rotation. Considering that the fuselage is proposed to be a body of rotation, the free stream angle of attack α and the free stream angle of sideslip β shall influence the drag coefficients in equal terms. Hence, the fuselage angle of attack α_{fu} is defined as the angle between the axis of rotation and the free airflow. Aligning the $\vec{x}_f$-axis with the axis of rotation, the formulation of α_{fu} is simply

$$\alpha_{fu} = \cos^{-1}\frac{u_{A,f}}{V_{A,f}}. \tag{2.20}$$

The fuselage drag coefficient is referenced to the freestream dynamic pressure $\frac{\rho}{2}V_A^2$ as well as the fuselage frontal area S_{fu}. Therefore, fuselage drag is calculated by

$$D_{fu} = \frac{\rho}{2} \cdot V_A^2 \cdot S_{fu} \cdot C_{D,fu}. \tag{2.21}$$

Since the fuselage drag is assumed to act at the aircraft's CG, and no further aerodynamic moment contributions by the fuselage are considered, the total moment of the fuselage acting on the aircraft's CG remains trivial; $\vec{M}_{A,fu} = 0$. Furthermore, the direction of the aerodynamic force $\vec{F}_{A,fu}$ contributed by the fuselage is gained by aligning the fuselage drag D_{fu} into the direction opposing the free stream velocity.

$$\vec{F}_{A,fu} = \begin{cases} -\frac{\vec{V}_A}{V_A} \cdot D_{fu} & V_A \neq 0 \\ 0 & V_A = 0 \end{cases} \tag{2.22}$$

Now that the aerodynamic forces and moments caused by all lifting surfaces and the fuselage are known, the total aerodynamic forces and moments acting on the aircraft are gained by simple summation.

$$\vec{F}_A = \vec{F}_{A,ls} + \vec{F}_{A,fu} \tag{2.23a}$$

$$\vec{M}_A = \vec{M}_{A,ls} + \vec{M}_{A,fu} \tag{2.23b}$$

2.2.5 Flight Control Kinematics

Each panel of every lifting surface is declared to be one of seven possible flight control surface types. Depending on the type of control surface, the flap deflection angle is determined as a function of longitudinal and lateral stick displacement η and ξ, rudder pedal position ζ as well as flap control handle setting κ.

Index	Flight Control Surface	Flap Deflection Angle	Actuated by
0	No Control Surface	–	–
1	Elevator	δ_e	η
2	Left Outer Aileron / Flaperon	$\delta_{a,l}$	ξ, κ
3	Left Inner Flaperon / Flap	$\delta_{k,l}$	ξ, κ
4	Right Inner Flaperon / Flap	$\delta_{k,r}$	ξ, κ
5	Right Outer Aileron / Flaperon	$\delta_{a,r}$	ξ, κ
6	Rudder	δ_r	ζ

Table 2.1: Types of Flight Control Surfaces

The flap deflection angles of each flight control surface are determined through the use of lookup tables and interpolation. Also, the definition of inner flaperons / flaps are optional within a given model, whereas the remaining surfaces are required for the simulation.

3 Validation of Models and Checks of Plausibility

In order to gain a more thorough understanding of the precision and limitations of any mathematical model of a physical process, comparison to experimental results is compulsory. This process is known as validation and allows for the determination of the limits to where the given model is still applicable. Furthermore, if no experimental data is available, any such mathematical model can still be checked for plausibility to see if certain phenomena occur in accordance with physical logic and experience. Before attempting to validate the aerodynamic models of chapter 2, a brief discussion of the required input parameters is in order.

3.1 Required Input Parameters

Any mathematical model of a physical process requires a given number of input parameters in order to provide mathematical results. The precision of the results, or output parameters, is not only dependent on the precision of the model itself, but also on the precision of the input parameters. The input parameters for the presented aerodynamics models can be grouped into several categories.

Aircraft Geometry being the location, orientation and airfoil of each different panel of all lifting surfaces

Airfoil Characteristics required are lift, drag and pitching moment coefficients of each airfoil

Fuselage Aerodynamics are represented by fuselage drag coefficients

CG Location in 3D

While working with the aerodynamic models of chapter 2, it has been found that particularly the airfoil coefficients have a significant influence on the precision of the simulation results.

3.2 Test Aircraft: The Schweizer SGS 1-36 Sprite

Of course, validation requires the input parameters of an actual test aircraft for which experimental results are available. Due to the constraints of this thesis, no experimental testing was possible, bringing up the demand that all required input parameters are freely available or can be easily determined otherwise. At the same time, it should be a representative aircraft, being similar to other aircraft which are to be analyzed with the presented aerodynamics models in the future.

One such aircraft which meets these demands is the US-produced Schweizer SGS 1-36 Sprite sailplane of figure 3.1. It is an all-metal design which made its maiden flight in 1979. Due to the fact that a modified Schweizer SGS 1-36 has been used by the *National Aeronautics and Space Administration* (NASA) for deep stall research[1], flight test reports by SIM [32] and by MAHDAVI and SANDLIN [23] are publicly available. Furthermore, Johnson [17] conducted independent flight testing.

[Source: NASA]

Figure 3.1: NASA's Schweizer SGS 1-36 Research Sailplane in Flight

3.2.1 Method of Gathering Input Data

Once the aircraft type for validation is decided upon, the groups of input parameters of section 3.1 are to be gathered. The aircraft's lifting surface geometry and aircraft dimensions as well as information on the different coordinate systems can be taken from the mentioned flight test reports of SIM [32] and MAHDAVI and SANDLIN [23] as well as the aircraft's Pilot's Operating Manual [31]. These sources also provide information on typical CG locations as well as the corresponding certified limits.

Fuselage information is much more sparse. Yet it is assumed that ALTHAUS' "ellipsoidal" fuselage from reference [5] represents the actual fuselage with enough precision. While this fuselage form is not rotationally symmetric anymore, ALTHAUS does not provide any data on the influence of the angle of sideslip β. Therefore, the fuselage is still treated as a body of rotational symmetry, which is a further simplification. The geometry and fuselage information allows aircraft's geometric model to be sketched in figure 3.2.

The by far most painstaking input data to be gathered are the airfoil aerodynamic coefficients. The Schweizer SGS 1-36's lifting surfaces sport three different airfoils, some with different flap geometries. These airfoil and flap combinations are as follows:

[1]Note the variable incidence horizontal tailplane for deep stall research. This feature is not installed production aircraft of the type and therefore has not been modeled.

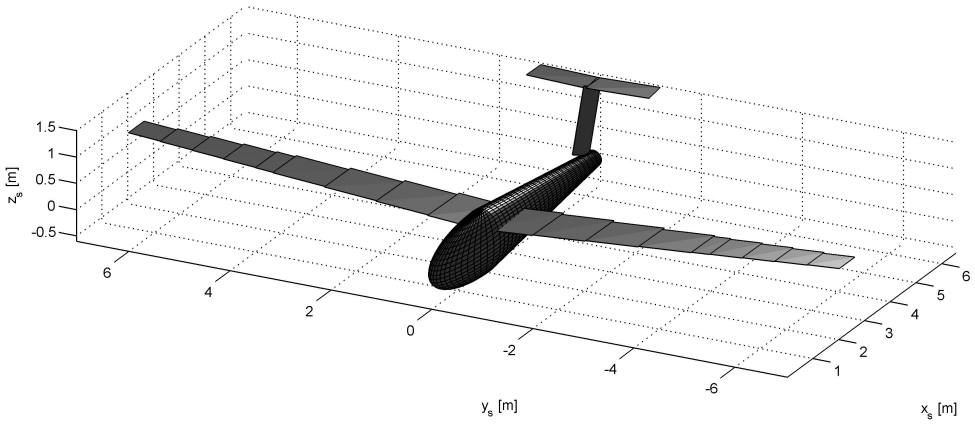

Figure 3.2: Sketch of the SGS 1-36 Geometry

FX 61-163 at the inboard main wing

FX 60-126 including a plain trailing edge flap of 25% chord as aileron at the outboard main wing

NACA 64_1-012 including a plain trailing edge flap of 35% chord as elevator at the horizontal stabilizer

NACA 64_1-012 including a plain trailing edge flap of 50% chord as rudder at the vertical stabilizer

It is proposed that all airfoil coefficients should be available for an airfoil angle of attack range of $\alpha \in [-10°, +20°]$. Experimental wind tunnel measurements for this AOA range as well as for all required flap settings of both Wortmann FX 60-126 and FX 61-163 airfoils are provided by Althaus and Wortmann [6].

While experimental measurements on a NACA 64_1-012 are principally available, they could not be utilized for a lack of the proper flap geometry which is used in the SGS 1-36 sailplane's stabilizers. Therefore it is necessary to predict the parameters by making use of a traditional aerodynamic code. For this case, the XFOIL code - embedded into the XFLR5 v. 5.00 [2] - is used.

Looking at the predicted lift and moment coefficients of the airfoil-flap combination of the horizontal stabilizer, the method's limits become quickly apparent. These coefficients are illustrated in figure 3.3. It appears that at an absolute flap deflection angle of $|\delta| = 10°$, the lift and moment coefficients are not fully symmetric, though the airfoil itself features a symmetric geometry. This already hints to stability issues of the algorithms implemented in XFLR5. Particularly, the predicted family of curves corresponding to flap deflections of more than $|\delta| = 10°$ frequently feature sharp edges and appear to be not completely differentiable within the studied AOA interval. Also, traditional two-dimensional panel methods have only a very limited

capability to depict the separated flow conditions which occur at high AOAs and/or at medium to large flap deflections. While the predicted coefficients appear to be plausible over the full AOA interval studied for small flap deflections, any deflection of $|\delta| \gtrsim 10°$ should cause concern about the precision of results. These issues are suspected to be aggravated by the larger flap of the vertical stabilizer.

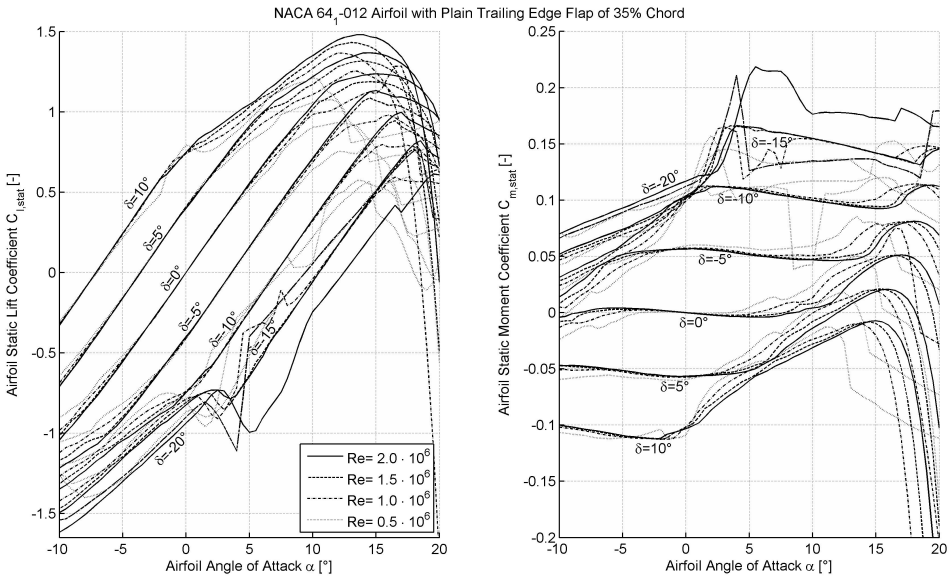

Figure 3.3: Selected Airfoil Coefficients Predicted by XFLR5

3.3 Validity and Plausibility

Unless otherwise noted, all calculations for the checks of validity and plausibility are carried out during stationary flight and out of ground effect (OGE) in standard conditions at sea level as prescribed by the ISA. No-wind conditions are presumed to exist. Due to restrictions on time available for the thesis and its scope - as well as a lack of experimental data - only the longitudinal motion of aircraft is studied.

3.3.1 Flight Performance and Stability of Longitudinal Motion

The quantitative part of JOHNSON's flight test of the Schweizer SGS 1-36 [17] focuses on the determination of the aircraft's polar. For this, he uses a calibrated pitot-static system to evaluate airspeeds and descent rates. Though this approach is very cost-effective, it is also very susceptible to atmospheric disturbances, a fact which he explains in reference [18].

A comparison between simulated and measured polars of the SGS 1-36 is provided in figure 3.4. Simulations have been carried out for $Re = 1.0 \cdot 10^6$ and $Re = 2.0 \cdot 10^6$. The Reynolds Number for all flight tests remains undefined. One could easily interpret that for both Reynolds Numbers the induced drag above the

lift coefficient for the best glide condition is slightly underestimated by the simulation. However, due to the atmospheric disturbance during experienced in all days of the flight test campaign, the measured polar cannot be assumed be of a fidelity high enough to allow such conclusion. This also serves to explain the "kink" in the experimental polar for aircraft lift coefficients $C_L < 0.5$.

Looking at the zero-lift aircraft drag coefficient[2] C_{D0}, one sees that this form of drag is somewhat underestimated by the simulation, particularly for the higher Reynolds Number. This seems logical when considering the fact that no parasite drag sources such as antennae, rivets and landing gear or interference drag at the fuselage-wing junction have been modeled.

Best glide performance for the SGS 1-36 is experimentally measured to provide a maximum glide ratio $E_{\max} \approx 31$ at a freestream airspeed of $V(E = E_{\max}) \approx 21\,\mathrm{m/s}$ calibrated airspeed for the given aircraft mass. For $Re = 1.0 \cdot 10^6$ the maximum glide ratio is simulated to be only 6% below the flight test results, and occurs at an airspeed 5% above the experiment. In the case of $Re = 2.0 \cdot 10^6$ these values change to 2% above experimental $E_{\max}$-results and 13% above experimental best-glide speed measurements.

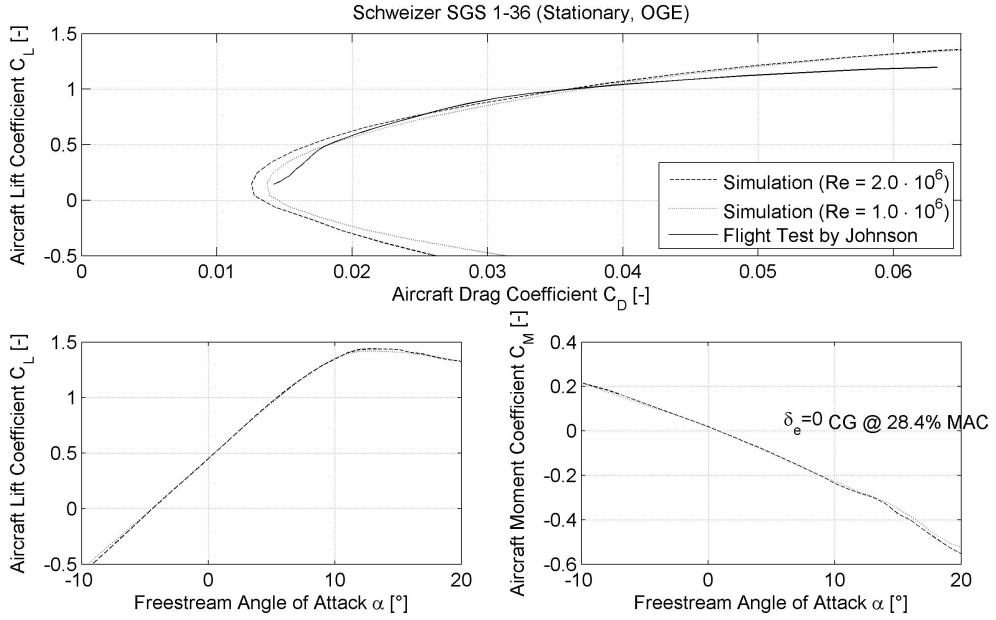

Figure 3.4: Flight Performance and Stability Parameters of the SGS 1-36

When studying the plot of C_L-vs-α in figure 3.4, the simulated results correspond well with experience. The zero-lift angle of attack varies between $\alpha_0 = -4.5°$ for $Re = 1.0 \cdot 10^6$ and $\alpha_0 = -4.4°$ for $Re = 2.0 \cdot 10^6$. Similarly, the maximum lift coefficients are calculated to be $C_{L\max} = 1.42$ and $C_{L\max} = 1.44$ correspondingly. After having passed $C_{L\max}$, lift only gradually reduces with further increases in angle of attack, which hints to the benign stalling characteristics reported by JOHNSON [17]. Though the aerodynamic coefficients for $\alpha \geq \alpha(C_{L,\max})$ need to be regarded with care. At this state flow separation already exists and - as described in section 2.2.2 - the predicted flow conditions are only a rough estimate.

[2] which for the flight test data would need to be extrapolated

Generally speaking, the plot of C_M-vs-α indicates a stable aircraft. For a fixed and neutral elevator deflection $\delta_e = 0$ and the CG being at 28.4% MAC the aircraft's zero-lift moment coefficient is positive; $C_{M0} > 0$. Longitudinal stability for a conventionally designed aircraft requires a negative gradient of $\frac{\partial C_M}{\partial \alpha} < 0$ besides a positive zero-lift moment coefficient $C_{M0} > 0$. This is predicted to be the case over the full studied AOA interval. At the same time, the numeric values of the predicted moment coefficient C_M have to be challenged as the influence of the aircraft's fuselage is completely unknown.

3.3.2 Controllability of Longitudinal Motion

The longitudinal motion of an aircraft is controllable if for any given airspeed, a corresponding elevator deflection δ_e can be selected to neutralize any pitching moment C_M at that speed, without an inadequate control force being required to do so. At the same time adequate control authority must still be present to the pilot to allow for maneuvering at this speed.

For validation of the simulation for controllability purposes, a look at the correlation between elevator flap deflection δ_e and the corresponding stationary freestream AOA α is taken. This is done by finding an appropriate elevator deflection to balance the pitching moments C_M caused by a given angle of attack. Control deflections for two different CG locations, for which experimental data was available from SIM [32], are studied. The results of this are presented in figure 3.5.

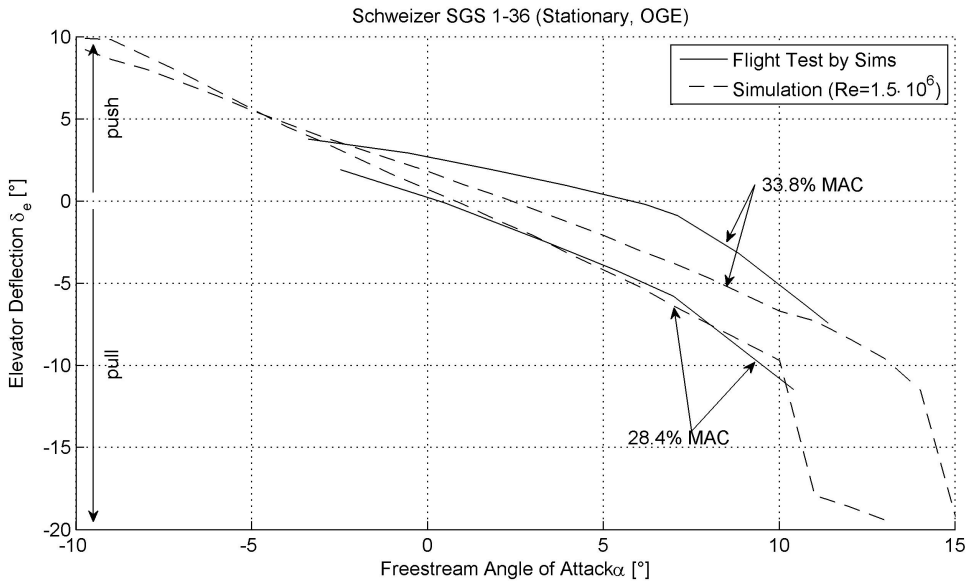

Figure 3.5: Correlation between Elevator Deflection and AOA for Trimmed Flight

One can see that experimental measurements of the elevator deflections to achieve trim are reproduced adequately only for some conditions. At the same time several phenomena are well depicted. The flight test data indicates that a rearward shift of CG will reduce the required (negative) elevator deflection as expected; $\frac{\partial \delta_e}{\partial x_{CG,s}} > 0$. However, the magnitude of $\frac{\partial \delta_e}{\partial x_{CG,s}}$ appears to be underestimated by an approximate factor of two in the simulation. At the same time, the simulated and

actual flight test curves have a negative gradient of $\frac{\partial \delta_e}{\partial \alpha} < 0$. The mean gradient of over the experimental interval is well predicted, yet the simulated curvature $\frac{\partial^2 \delta_e}{\partial \alpha^2}$ is greatly underestimated. The large drops in simulated elevator deflection at high angles of attack are associated with XFLR5 predicting a stall of the elevator airfoil at the corresponding Reynolds Number, flap deflection and local angle of attack.

By keeping in mind that an increase in AOA causes a decrease in airspeed for trimmed flight ($\frac{\partial \alpha}{\partial V} < 0$), we know that for the entire simulated and measured range the expression of $\frac{\partial \delta_e}{\partial V} > 0$ is valid. This fact is often demanded by common certification regulations, such as CS 22.173(a)(2) [12].

> "The slope of the curve, stick displacement versus speed, must not be negative, except that a negative slope may be acceptable provided that it can be demonstrated that there is no difficulty in control."

The fact that for a given CG the simulated and (extrapolated) experimental curves run at some distance to one another at the zero-lift AOA α_0 can be interpreted as follows: A different elevator deflection is required to balance both zero-lift moment coefficients C_{M0}, indicating that these moment coefficients are of different magnitude. The primary difference between the two is the fact that the zero-lift moment calculated in the simulation does not regard the moment created by the fuselage. Hence, the moment contribution of the fuselage is of some importance.

By knowing that the mean gradients of the δ_e-vs-α curves over the examined AOA interval are of similar magnitude indicates that the elevator authority is also similar. The simulated elevator does not prematurely or belatedly reach its maximum deflection in comparison to the flight test results. Consequently, the longitudinal controllability of the simulation is granted.

Downwash Angle Estimation

To gain further understanding of the errors in the simulated wake structure the downwash angle ε_h at the horizontal stabilizer is studied. Wake errors might be partially responsible for the false prediction of the curvature of the δ_e-vs-α plot. This study is most easily done by formulating the aircraft's pitching moment coefficient C_M analogous to the lectures of Alles [4].

$$C_M = C_{M0,\delta e=0} - \frac{x_{AC} - x_{CG}}{c_{\text{mac}}} \cdot C_L(\alpha) - \underbrace{\frac{x_h - x_{CG}}{c_{\text{mac}}} \cdot \frac{p_{\text{dyn,h}}}{p_{\text{dyn}}} \cdot \frac{S_h}{S_{\text{ref}}}}_{=V_h} C_{Lh}(\alpha_h, \delta_e) \quad (3.1)$$

Here $C_{M0,\delta e=0}$ describes the zero-lift moment coefficient experienced by the aircraft without deflected elevator and is a function of the CG location. The relative position of the aircraft's aerodynamic center to its CG is $\frac{x_{AC}-x_{CG}}{c_{\text{mac}}}$ with an analogous formulation for the aerodynamic center of the horizontal stabilizer $\frac{x_h-x_{CG}}{c_{\text{mac}}}$. Equation 3.1 assumes that the total aircraft lift $C_L(\alpha)$ acts in the aircraft's aerodynamic center and the lift $C_{lh}(\alpha_h, \delta_e)$ of the horizontal stabilizer is a function of the horizontal stabilizer's local angle of attack α_h and elevator deflection δ_e. It only serves to influence the aircraft's pitching moment. The dimensionless product of the relative stabilizer location, the ratio of local stabilizer and global dynamic pressures $\frac{p_{\text{dyn,h}}}{p_{\text{dyn}}}$ and ratio

of horizontal stabilizer and reference areas $\frac{S_h}{S_{\text{ref}}}$ is known as the horizontal stabilizer volume coefficient V_h, as defined in equation 3.1.

By assuming the stabilizer lift coefficient to remain within the linear realm of aerodynamics, we can superpose the influences of the elevator deflection and the local angle of attack.

$$C_{Lh}(\alpha_h, \delta_e) = C_{Lh\alpha h} \cdot (\alpha_h - \alpha_{h0}) + C_{Lh\delta e} \cdot \delta_e \tag{3.2}$$

The inclusion of a zero-lift stabilizer angle of attack α_{h0} allows non-symmetric stabilizer airfoils to be regarded.

We further know that the horizontal stabilizer AOA α_h is a superposition of the freestream AOA α, the downwash angle ε_h and the horizontal tailplane incidence i_h in linear studies.

$$\alpha_h = \alpha - \varepsilon_h + i_h \tag{3.3}$$

By assuming that the aircraft is in trimmed flight ($C_M = 0$) and combining the previous equations 3.1 through 3.3 we arrive at a linear formulation for ε_h.

$$\varepsilon_h = \alpha + i_h - \alpha_{h0} - \frac{1}{C_{Lh\alpha h}} \left[\frac{1}{V_h} \left(C_{M0,\delta e=0} - \frac{x_{AC} - x_{CG}}{c_{\text{mac}}} \cdot C_L(\alpha) \right) - C_{Lh\delta e} \cdot \delta_e \right] \tag{3.4}$$

To compare the downwash angles predicted by the simulation and those experienced during the flight tests of SIM [32], $\delta_e(\alpha)$ is taken from figure 3.5. All other parameters are estimated using the simulation results. The results of equation 3.4 evaluated for the available cases is provided in figure 3.6.

We can see that for the CG at 28.4%MAC that the downwash angle at the horizontal stabilizer is predicted with an absolute precision of approximately 1°. For this case the gradient $\frac{\partial \varepsilon_h}{\partial \alpha}$ is within 12% of experimental results[3]. However, the theory presented above indicates that for the CG being at 33.8%MAC, the gradient of $\frac{\partial \varepsilon_h}{\partial \alpha}$ is underpredicted by about 52%. Above $\alpha \gtrsim 5°$ the theory is not applicable due to the horizontal stabilizer lift coefficient leaving the domain where the linear superpositions of equation 3.2 are valid.

The great span of precision in which the elevator downwash appears to be predicted is somewhat unsettling. Considering that the absolute errors for the forward CG location are relatively small it seems plausible that other sources of errors might be responsible for the deviation between simulated and experimental results in figure 3.5.

Though not illustrated in figure 3.6, it has been demonstrated that variations in the ratio of dynamic pressures $\frac{p_{\text{dyn,h}}}{p_{\text{dyn}}}$ as well as in the horizontal stabilizer lift parameters $C_{Lh\alpha h}$ and $C_{Lh\delta e}$ are only of secondary influence[4]. They do not alter the path of the $\varepsilon_h(\alpha)$-plots noticeably.

Another source of error with greater effect might be a falsely determined relative distance between the aircraft's aerodynamic center and its CG. This factor is much greater and could easily be responsible for the deviations.

Considering that the vertical stabilizer is perpendicular to the main wing, its angle of attack in symmetric flight is not directly influenced by the main wing's downwash. Therefore it is not prone to the error effects discussed above.

[3] The mean gradient is determined in the interval of $-2° \leq \alpha \leq 5°$

[4] Such variations might have been the results of improper parameter estimation.

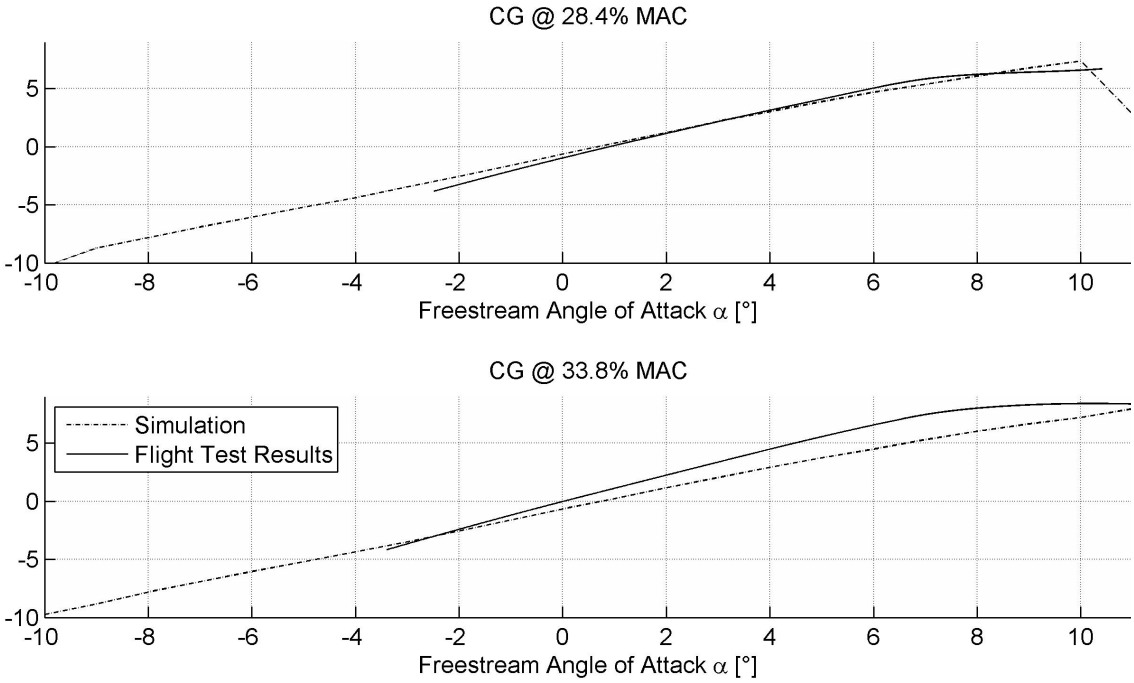

Figure 3.6: Experimental and Simulation Results of the Downwash Angle ε_h at the Horizontal Stabilizer

3.3.3 Instationary Effects

As indicated before, it is suspected that dynamic effects have a notable influence in several winch launch accidents. Therefore, is important to include corresponding dynamic models in the simulation. Unfortunately, no proper data for validating the dynamic models is available, making only checks of plausibility possible.

In order to study the behavior of dynamic lift effects, the simulated aircraft is exposed to pitch oscillations around its CG at a constant airspeed $V_A = 22.5\,\mathrm{m/s}$ while being in symmetric free flight (OGE). This leads to temporal changes in the angle of attack α.

$$\alpha(t) = \bar{\alpha} + \hat{\alpha} \cdot \cos(2\pi \cdot f \cdot t) \tag{3.5}$$

$\bar{\alpha}$ denotes the mean AOA, which is retained constant at $\bar{\alpha} = 5°$ for the study. Furthermore, $\hat{\alpha}$ is the amplitude of the AOA oscillation and is varied between $\hat{\alpha} = 1°$ and $\hat{\alpha} = 10°$. The results are also evaluated for different frequencies $f = 0.20\,\mathrm{Hz}$ and $f = 2.00\,\mathrm{Hz}$. The temporal function of the aircraft's pitch speed q_A is easily taken from equation 3.5.

$$q_A(t) = -2\pi \cdot f \cdot \hat{\alpha} \cdot \sin(2\pi \cdot f \cdot t) \tag{3.6}$$

All calculations are performed for a Reynolds Number of $Re = 1.5 \cdot 10^6$ as well as a CG location of 28.4% MAC. These settings lead to the dynamically variant lift coefficients presented in figure 3.7.

The most prominent difference between the static lift coefficient and the lift coefficients in dynamic flight is the inclusion of a lift hysteresis. Such effects are

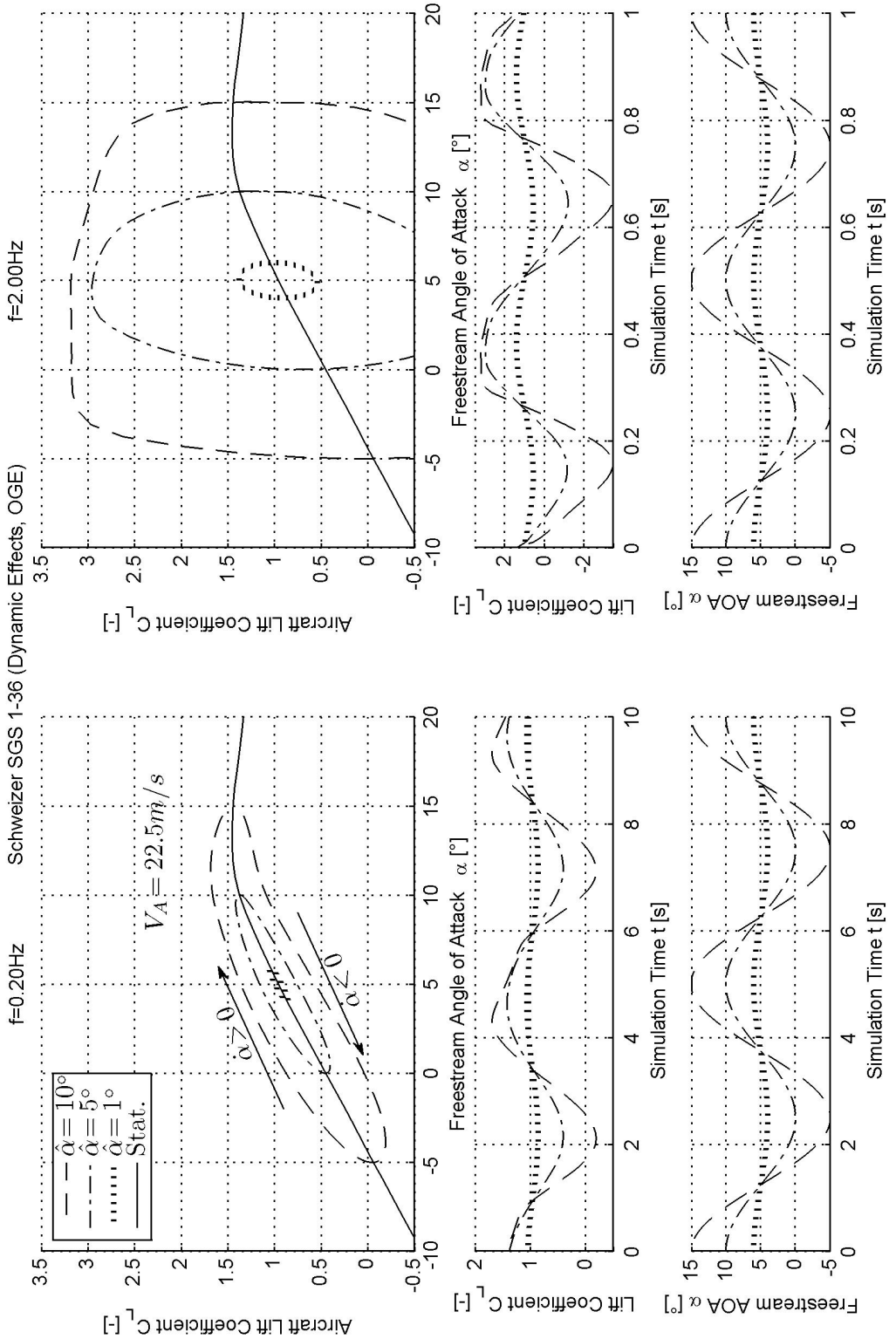

Figure 3.7: Prediction of Dynamic Lift Effects

seen in the C_l-vs-α plots of figure 3.7. The primary cause of the hysteresis is equation 2.4, with wake effects being only of extremely limited magnitude. Main factors influencing the intensity of the hysteresis are frequency and amplitude of the AOA oscillation, which define the maximum temporal change in the angle of attack $\dot{\alpha}_{\max} = 2\pi \cdot f \cdot \hat{\alpha}$.

When studying the C_l-vs-α plots further, a plateau can be noted for the case of $f = 2.00\,\text{Hz}$ and $\hat{\alpha} = 10°$. The mathematical cause of this is that the panels' local lift coefficients reach the boundaries defined in equation 2.4. Physically this is a formulation of the fact that lift will not be infinitely increased by raising $\dot{\alpha}$. Yet, at first it seems somewhat unusual that the aircraft's maximum lift coefficient $C_{L,\max}$ for this case is greater than the maximum instationary airfoil lift coefficient $C_{l,\text{inst},\max} = 3$ of equation 2.4. However, this effect can be traced to the significant pitch speeds q_A. These raise the local AOA α_h and dynamic pressures $p_{\text{dyn},h}$ at the horizontal stabilizer notably. This effect serves to raise horizontal stabilizer and total aircraft lift, which then is normalized by the freestream dynamic pressure p_{dyn} and aircraft reference area S_{ref} to create the total aircraft lift coefficient C_L.

By comparing the plots of lift coefficient C_L and angle of attack α versus simulation time t, one notes that C_L leads before α. This, of course is to be expected, considering that C_L depends on two different terms, one being a function of α and the other being a function of $\dot{\alpha}$. If one stays within the quasi-linear branch of the C_L-vs-α plot and the magnitude of $\dot{\alpha}_{\max}$ is small enough to prevent C_L from plateauing, C_L can be described of being a PD-function (proportional and differentiating) of α. One of the mathematical consequences of this formulation is that the lead angle ϕ, by which changes in lift precede changes in AOA, is only a function of the frequency f, see Abel [3].

3.3.4 Ground Effect

Considering that a number of loss-of-control incidents and accidents during the winch launch occur in proximity to the ground it seems prudent to include a ground effect model in the simulation. Experience indicates that an aircraft within approximately one wingspan of the ground[5] will experience notable changes in trim and will have a tendency to "float", indicating a significant increase in glide ratio. Physically, the presence of the ground hampers the development of the induced velocities created by a lifting surface's vortex sheet. Instead, the induced downwash velocities are reduced and therefore decrease induced drag. In the mathematical models of chapter 2 these effects are created by presuming the ground to be a mirror plane and mirroring the full vortex distribution describing the aircraft and its wake.

For analysis the aircraft once again is simulated in a stationary and symmetric flight condition with a Reynolds Number of $Re = 1.5 \cdot 10^6$ and a CG location of 28.4% MAC. The AOA is held constant at $\alpha = 5°$ as the aircraft moves parallel to the ground. Unfortunately, for operations in ground effect (IGE), no test data is available either in the reports studied, therefore only allowing for a further check of plausibility. The aircraft's height h is varied between ground level and one wingspan above the ground. Relative changes of the lift coefficient $\Delta C_L / C_{L,\text{OGE}} = \left(C_{L,\text{IGE}} - C_{L,\text{OGE}}\right) / C_{L,\text{OGE}}$ are determined as a function of the air-

[5] such as during takeoff and landing

craft's relative height h/b above the mirror plane. Analogous relative changes are determined for the drag coefficient, pitching moment coefficient and glide ratio. The corresponding values are presented in figure 3.8.

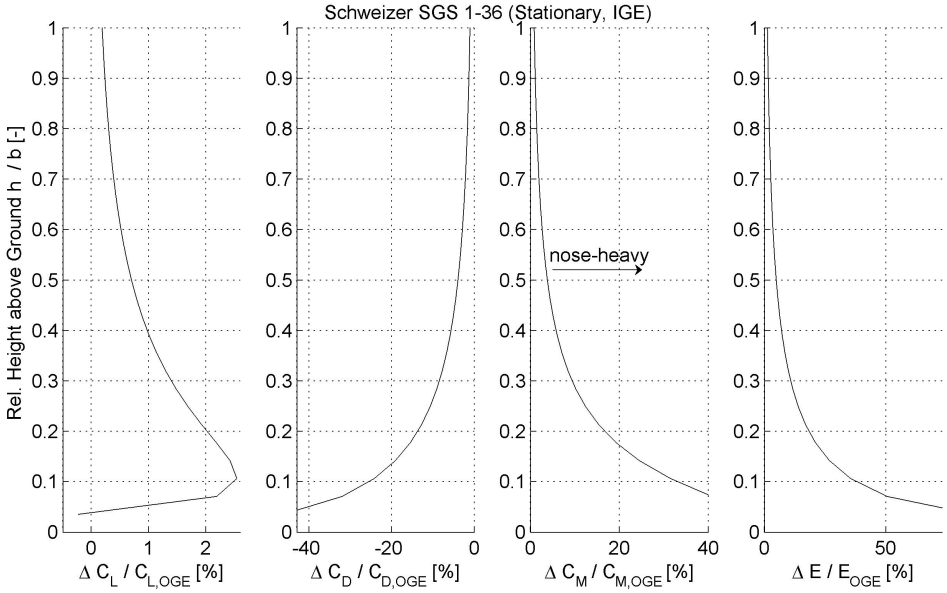

Figure 3.8: Influence of Ground Effect on the Aircraft

When studying these effects, one sees that changes in the lift coefficient C_L are of a negligible magnitude as the aircraft approaches the ground plane. Flight experience shows that an aircraft's stall speed does not vary notably on takeoff or landing, therefore supporting the only minor changes in lift coefficient.

Much more notable changes apply to the aircraft's drag coefficient C_D. It is significantly reduced by the presence of ground effect. While no experimental data on the influence of ground effect on drag of the SGS 1-36 is available, a brief glance into the flight operations of powered aircraft serves to illustrate that ground effect has a major influence on drag. A commonly used short-field takeoff technique in powered flight operations calls for the pilot to lift the aircraft off the ground as soon as possible. Then, the aircraft shall be kept at a minimal height above the runway to accelerate as quickly as possible to the airspeed for the best angle of climb. Only then should the pilot initiate the actual takeoff climb.

Another expression of the reduced drag in ground effect is the prolonged "floating" of an aircraft during the flare to landing. Particularly prone to this phenomenon are gliders in low wing configuration or aircraft with a high aspect ratio. Of course, the large reductions in the drag coefficient at low height will increase the glide ratio $E = C_L/C_D$.

While changes in drag and glide ratio primarily influence the aircraft's flight performance the influences on aircraft stability and control are also of interest. RAYMER [27] states that an aircraft in ground effect will experience a significant change in pitch trim, with the aircraft becoming "nose-heavy". This requires a larger deflection of the elevator[6] than would be necessary in free flight in order to balance the aircraft's pitching moment.

[6] by further pulling on the control stick

An explanation of this phenomenon is provided by studying the effects of the induced velocities. As the aircraft approaches the mirror plane, the downwash angle ε_h at the horizontal stabilizer is reduced. This leads to the higher local angles of attack at the stabilizer, thereby increasing the nose-down moment. Figure 3.8 describes this increase in pitch-down moment and is in correlation with RAYMER's statement.

3.3.5 Summary of Model Validity

Summing up the results of the validation and checks of plausibility one can say that the developed aerodynamics models depict those phenomena which are suspected of playing an important role in winch launch accidents. Principally, the aerodynamic performance over a large part of the stationary flight envelope appear to be predicted with a very acceptable degree of accuracy. However, the wake model can only be considered a first-order engineering estimation in the proximity of stalled flight.

For the validated glider type control effectiveness is predicted in the same order of magnitude as that of the real aircraft. Shortcomings, which were originally attributed to errors in the wake structure might have also be caused by false parameter estimations for the rear CG position. Yet as far as the source responsible for the deviations in the trim curve for rear CG locations remain unidentified a certain degree of scientific caution is in order.

While the flight performance and control aspects in stationary free flight and out of ground effect are able to be validated, no such opportunity is given to the influences of dynamic behavior and ground effect. Yet, the models implemented appear to provide plausible results which concur with experience. All in all, it is adequate to say that the aircraft is simulated with a behavior that is "similar" to the actual aircraft. This implies that not all aerodynamic effects are simulated at high fidelity but the phenomena of interest are depicted in a way to allow them to be studied.

4 Software Integration

In order to be used with the 6DoF winch launch simulation environment of the *Institute of Flight System Dynamics*, the aerodynamic modeling presented and validated within the previous chapters of this thesis are integrated into the corresponding Simulink model. As most of the necessary code has already been written as MATLAB functions, these are incorporated into an embedded MATLAB routine which calculates the aerodynamic forces and moments acting on the given aircraft as a function of its position, attitude and velocities. The initialization routines and circulation converger are still run as regular MATLAB scripts during the initialization of the Simulink `Aerodynamics` block.

However, rewriting the validated code to stay within the embedded MATLAB subset of functions proved to be strenuous and time-consuming. At the same time, the risk of introducing new errors to the code rises with the necessity for restructuring existing functions. The R2010a release of MATLAB/Simulink features several major improvements over previous versions which reduced the demand for restructuring existing code. Namely these improvements are that embedded MATLAB now allows for variable size data in embedded blocks as well as for the use of logical indexing.

4.1 Restrictions on Aircraft Model

Due to the limitations on passing variable size data within Simulink, several restrictions apply to the models presented in chapter 2. These are that the 6DoF model aircraft must have exactly $n_{\mathrm{surf}} = 3$ lifting surfaces. Thereby the main wing must be attributed to $i_{\mathrm{surf}} = 1$ to allow for the correct determination of the total aircraft aerodynamic coefficients for the graphical user interface. Also, the total number of panels of all three lifting surfaces is limited to $\sum_{i_{\mathrm{surf}}=1}^{3} n_{\mathrm{pan}} \leq 50$.

4.2 Stability Problems

For the validation and checks of plausibility of chapter 3, the aerodynamics model is exposed to predefined motions of the aircraft. For these cases it has been possible to reach stable solutions of the lift distribution and wake intensity. However, by coupling the models of chapter 2 with the 6DoF equations of motion of the flight simulation, the wake and circulation distribution diverge within a very short timespan. Restabilizing the wake and circulation distribution proves to be cumbersome.

The cause of the destabilization of the wake when merging the aerodynamic models with the 6DoF equations of motion appear to be the influence of the time-dependent derivatives of the panel circulation $\dot{\Gamma}_{\mathrm{pan}}$ as well the local geometric angle of attack $\dot{\alpha}_{\mathrm{geo,loc}}$. A stable wake and circulation solution is only reached in the 6DoF

flight simulation when disregarding the influence of $\dot{\Gamma}_{\text{pan}}$. This is done by setting $k_{\text{circ}} = 0$ within equation equation 2.7.

It is also found that an even number of main wing panels is detrimental to wake stability. For an even number of main wing panels, a vortex is shed directly in the plane of symmetry, which then causes contrary changes in the adjacent panels. These asymmetric changes then propagate along the wingspan and cause further asymmetric vortices to be trailed from the main wing. A simple way of avoiding this scenario is by modeling the main wing with an uneven number of panels. This way the central panel trails its vortices not directly on the apex of the dyhedraled wing.

A further concern is of a more mathematical nature. To prevent an algebraic loop from being formulated around the embedded MATLAB block, $\alpha_{\text{geo,loc}}$ is differentiated outside of the block. Disruption of an algebraic loop is usually reached by delaying the signal flow by the magnitude of one timestep Δt, yet it was found that a larger delay of $k_{\text{delay}} \cdot \Delta t$ proved to provide better wake stability. With k_{delay} being the delay multiple of the simulation timestep size and s being the Laplace Variable the relationship between $\alpha_{\text{geo,loc}}$ and $\dot{\alpha}_{\text{geo,loc}}$ can be rewritten as

$$\dot{\alpha}_{\text{geo,loc}}(s) = k_{\text{fade}} \cdot \alpha_{\text{geo,loc}}(s) \cdot s \cdot e^{-k_{\text{delay}} \cdot \Delta t \cdot s}. \tag{4.1}$$

Here k_{fade} is an airspeed-dependent fading factor, which linearly introduces the $\dot{\alpha}_{\text{geo,loc}}$-dependency into the aerodynamic calculations between two airspeeds $V_{\text{fade,off}}$ and $V_{\text{fade,on}}$.

$$k_{\text{fade}} = \begin{cases} 0 & V_A \leq V_{\text{fade,off}} \\ \frac{V_A - V_{\text{fade,off}}}{V_{\text{fade,on}} - V_{\text{fade,off}}} & V_{\text{fade,off}} < V_A < V_{\text{fade,on}} \\ 1 & V_A \geq V_{\text{fade,on}} \end{cases} \tag{4.2}$$

This has become necessary due to the landing gear model. Since the landing gear is modeled as a spring, mass and damper system, minor vertical oscillations occur even as the aircraft stands still. These minuscule motions along the vertical axis would, however, cause the angle of attack to vary between $-90° \leq \alpha \leq 90°$. Due to the high frequency of these vibrations, the corresponding derivative are relatively high and, without being faded out, would cause the aerodynamic forces to reach unrealistic values at minor airspeeds.

Furthermore, high frequency oscillations of a small amplitude propagate from the wake to the aerodynamic forces and moments acting on the aircraft CG. Due to the rigid body assumption underlying the simulation the resulting high frequency motions directly serve to excite further oscillations in the wake. To alleviate this effect, the total aerodynamic forces and moments of the lifting surfaces $\vec{F}_{A,ls}$ and $\vec{M}_{A,ls}$ are passed through a lowpass filter. This can be interpreted as modeling the structural damping of high frequency aerodynamic oscillations.

5 Flight Mechanics of Winch Launch Accidents

Considering that a goal of this thesis is to provide a tool for future flight mechanics reconstruction of winch launch accidents, the presented aerodynamics models need to be evaluated on their aptitude of standing up to this task. For this evaluation a test case is proposed which is considered likely to result in stall-spin type accident scenario. In the past these low-level loss-of-control accidents with the glider rolling inverted rapidly and irrecoverably have resulted in a series of fatal accidents. The simulation results should by no means be interpreted as a full explanation of any accident. A high number of assumptions need to be made for this purpose, such as defining pilot flight control inputs, proposing acting wind conditions, etc. Much rather should the simulation results be used in the future to identify possible technical factors contributing to an accident.

In the process of defining the ensuing hypothetical accident scenario, a mechanism governing the interaction between aircraft behavior, launch safety and pilot behavior became obvious. This mechanism is most easily described in the form of a flight envelope, which is presented in the following section.

5.1 Flight Envelope During the Winch Launch

During the winch launch the aircraft's flight envelope underlies certain restrictions. Principally, the aircraft's airspeed V_A must be kept above the stall speed V_S and below the maximum winch launch speed V_W. Unbeknown to many pilots the stall speed is influenced by the vertical load factor, which has been previously discussed by the author [29]. As the aircraft rotates into the climb and the angle between the cable and the aircraft's longitudinal axis increases, the additional cable force in direction of the aircraft's vertical axis needs to be compensated by additional lift. This increases the effective load factor, thereby raising the stall speed initially. At the other end of the speed spectrum the maximum winch launch speed restricts operations. Yet while complying with the operating limitations is compulsory for the pilot, exceeding the maximum winch launch speed is not uncommon. Pilots tend to accept tow speeds in excess of the maximum placarded winch launch speed if this keeps the aircraft from transitioning into an excessively steep climb.

At the same time the pitch angle Θ, which is a control parameter directly perceivable by the pilot[1] during the launch, must be kept within limits. The upper limit of the pitch angle is restricted by the fact that during a rope break, the aircraft's nose must be lowered swiftly below the horizontal to transition into conventional soaring flight and keep an adequate margin against stalling. This pushover maneuver

[1] through the visual channel

must also regard the pilot's reaction time to perceive the rope break and initiate the recovery. The maximum permissible pitch angle rises with an increase in airspeed as more energy is available to conduct the pushover maneuver.

Also, a minimum pitch angle exists. At the low speed end of the flight envelope this is dictated by keeping the airplane from stalling. As airspeed increases, the operational demand of attaining a minimum (and safe) release altitude dictates that a minimum climb angle must be achieved. The boundaries of the flight envelope are illustrated in figure 5.1.

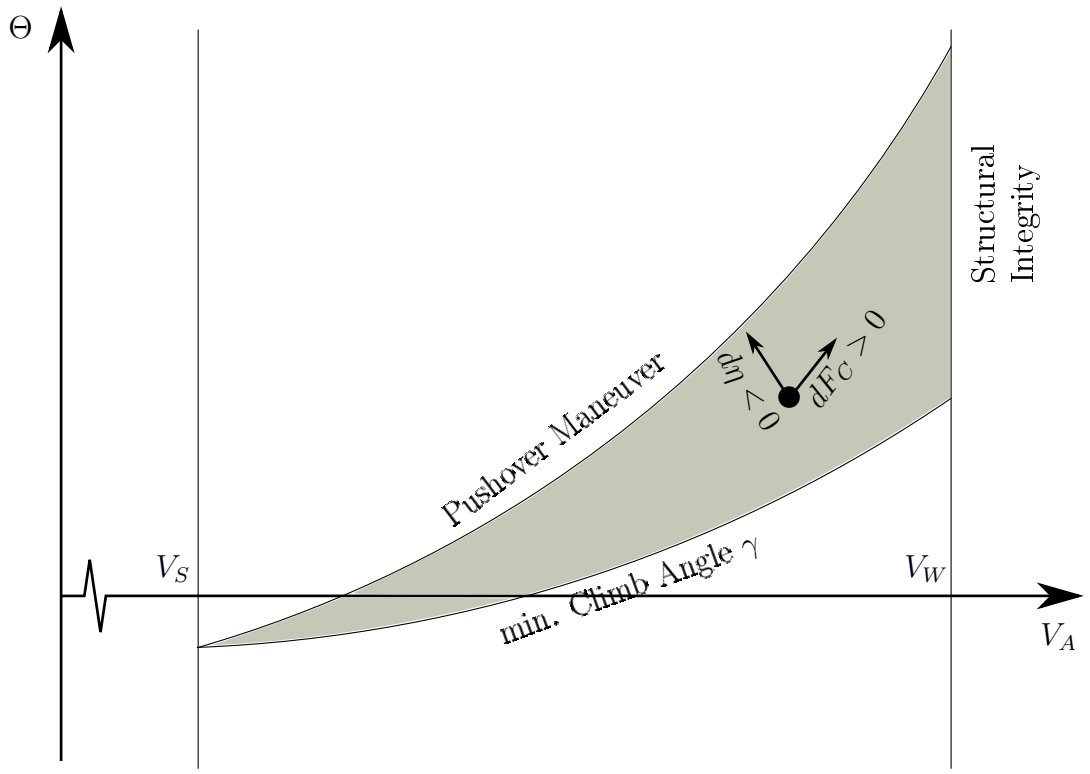

Figure 5.1: Flight Envelope During the Winch Launch

Whereas the speed boundaries should be explicitly known to the pilot after having studied the respective handbooks, the pitch boundaries are much more often gaged by experience. The diagram of figure 5.1 is not printed in any flight operation manual. Due to this, and to allow for adequate reaction times in the event of a cable break, most flight training curricula teach students to keep a notable safety margin to the boundaries, particularly the maximum pitch angle. Ideally, the glider's natural tendency during the launch will be to capture an operating condition within the center of the envelope during the initial launch. As a result the pilots actions would be kept to a minimum.

The location of this operating condition, of course, is influenced by a multitude of factors. Of particular interest are the possibilities of controlling the location of the operating condition. An increase in cable force acting on the glider $dF_C > 0$ can be controlled by the winch operator. This shifts the operating point into the direction of higher speeds as well as higher pitch attitudes. If the pilot decides to pull on the control stick $d\eta < 0$ then the aircraft will deviate from the operating

location in the direction of lower airspeeds and higher pitch angles. As the operating condition approaches the pushover boundary it can be assumed that the workload of the pilot rises. This is due to the fact that for a safe flight at higher pitch attitudes the pilot has to allot more concentration onto reacting swiftly in case of a rope break to initiate the pushover maneuver.

The behavior during the initial phase of the winch launch plays a central role in many of the studied accidents. This winch launch behavior and the actual path taken through the envelope is defined by the relationship of translational and rotational accelerations. These in turn are caused by the forces and moments acting on the aircraft at any given time. In the case of the initial winch launch phase just after lift-off, the moments and forces induced by the cable into the glider dominate. By assuming that the cable force F_C acts parallel to the aircraft's longitudinal axis in the initial phase, we determine longitudinal load factor $n_{C,x}$ induced by the cable to be

$$n_{C,x} = \frac{F_C}{m \cdot g} \tag{5.1}$$

Here m describes the aircraft's take-off mass and g is the gravitational acceleration. Similarly, the rotational acceleration around the lateral axis $\dot{q}_C$, caused by the cable force, can be assumed to be

$$\dot{q}_C = \frac{F_C \cdot r_{\text{CG-Hook},z}}{I_{yy}} \tag{5.2}$$

In this case $r_{\text{CG-Hook},z}$ describes the vertical distance between the tow hook of the glider and the aircraft's CG and I_{yy} is the moment of inertia around the pitch axis. Combining equations 5.1 and 5.2, as well as introducing the definition of the radius of gyration of the pitch axis $r_{g,yy} = \sqrt{\frac{I_{yy}}{m}}$, results in the ratio of pitching and normal accelerations, caused by the cable force.

$$\frac{\dot{q}_C}{n_{C,x}} = \frac{r_{\text{hook},z}}{r_{g,yy}^2} \cdot g \tag{5.3}$$

5.1.1 Motorgliders During the Winch Launch

While gathering the required data for chapter 1 there was the subjective impression of an overproportional representation of motorgliders[2] being involved in winch launch accidents. These aircraft designs are often derived from pure sailplanes by installing an extendable engine and/or extendable propeller in the aircraft's fuselage. For static stability purposes this installation is done close to the aircraft's CG. While this adds considerable mass to the aircraft, its moments of inertia are affected to a much lesser degree by the installation of the propulsion unit. As a consequence the radius of gyration $r_{g,yy}$ decreases in a motorglider conversion in contrast to its "pure" glider equivalent.

Flight performance during the initial winch launch (take-off distances, etc.) is primarily dictated by the acting longitudinal load factor $n_{C,x}$. When demanding the

[2] Within this thesis the term "motorglider" is used in the meaning of an auxiliary-powered sailplane and not as a touring motorglider (TMG). While auxiliary-powered sailplanes might be winch launched, TMGs are usually not provided with this possibility.

same take-off performance for a motorglider design as of the conventional sailplane variant, equation 5.3 requires that the motorglider will experience higher pitch accelerations during the initial winch launch due to its lower $r_{g,yy}$. As a consequence the aircraft operates closer to the upper flight envelope boundary. Figure 5.2 illustrates the qualitative paths that two derivates of the same aerodynamic glider design will take during the initial winch launch, one being a pure glider and the other being the motorglider with extendable propulsion unit. For a typical 18 m class glider, the radius of gyration $r_{g,yy}$ can decrease by $\approx 7\%$ with the installation of the propulsion unit, the necessary auxilliary equipment and operating fluids. This raises the ratio of m/I_{yy} by $\approx 15\%$. Particularly single-seat designs with their lower I_{yy} are more prone to this phenomenon than are twin-seat motorgliders.

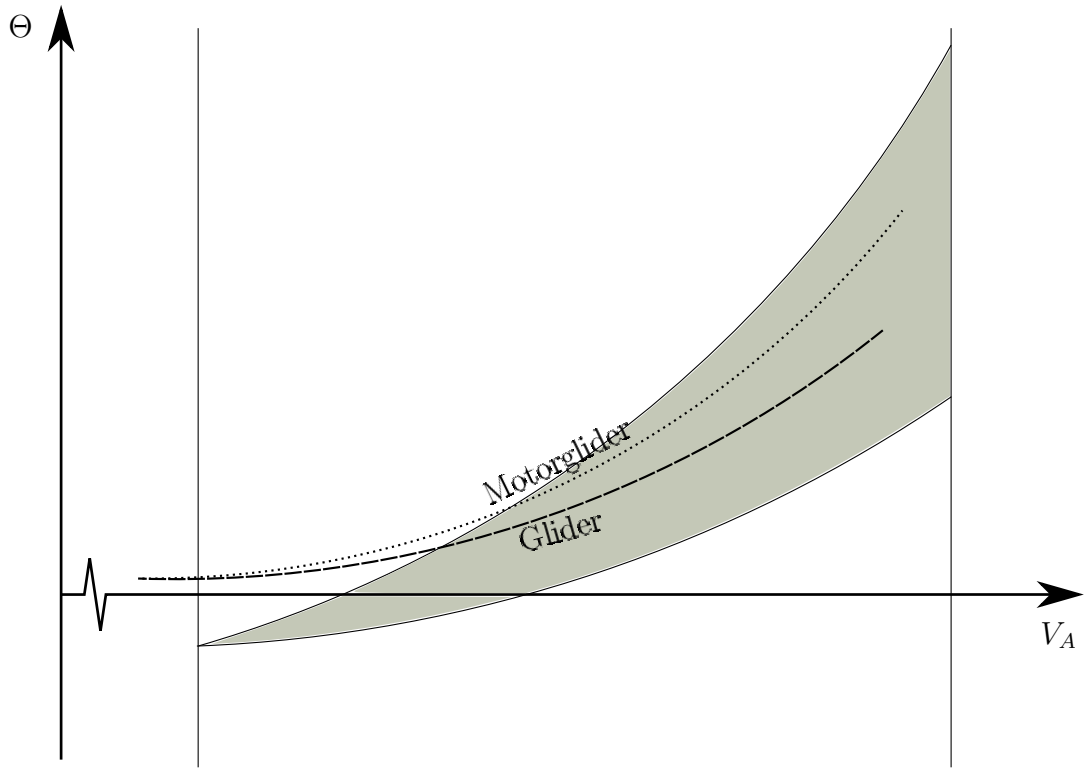

Figure 5.2: Flight Envelope Trajectories of a Pure Glider and Motorglider of the Same Aerodynamic Design

In the past motorglider conversions of an existing glider design have most often been treated as an extension of the existing type certificate. If the existing "pure" glider design has shown satisfactory performance during the winch launch then the motorglider derivative has also been certified for winch operations without any further flight testing required. This certification action is based on the assumption that the winch launch behavior of both designs is identical, due to their identical aerodynamic characteristics and the motorglider's longitudinal CG location staying within the certified limits of the "pure" glider variant. While this does pay tribute to the static balance of moments during the winch launch it has been shown above that the dynamic behavior is by no means identical. Aircraft manufacturers and certification authorities should be made aware of this fact.

5.2 A Hypothetical Accident Scenario

To determine the suitability of the developed aerodynamics models and the remaining winch launch simulation environment for accident reconstruction, a hypothetical accident scenario is developed. Due to the fact that high-performance motorgliders are more prone to the severe stall-spin type accidents, a generic model of such an aircraft has been implemented for this study. It is representative of an 18 m class motorglider with two trailing-edge flaperons per wing. A total of five flap settings ($F1$ through $F5$) are available to the pilot. The airfoils - being the basis for the BET model of the aircraft - are similar to the modern high-performance DU airfoils installed on the wings and stabilizers of several gliders of the 18 m class.

The simulated accident scenario consists of the following characteristics:

Mass and Balance Take-off mass $m = 495\,\mathrm{kg}$, CG location close to the center of the permissible envelope resulting in a static stability margin of $\frac{x_{AC}-x_{CG}}{c_{\mathrm{mac}}} = 0.325$

Airfield 1000 m tow distance, airfield elevation $\approx 600\,\mathrm{m}$

Meteorological Conditions no wind, warm summer conditions resulting in density altitude of 890 m

Cable synthetic cable[3]

Winch Force commanded winch force is 2000 N for the first 4 s of the simulation, then increased at a rate of $\approx 2000\,\mathrm{N/s}$ to 6000 N [4]

Winch Transmission actual winch force output is multiplied by a factor of 2.5 during the simulation time ranging from 5.0 s to 5.5 s [5]

Flight Controls all primary flight controls remain neutral, flaps are set to middle setting $F3$

One operational error, which is in contrast to typical procedures described in a flight operation manual, is also included.

Weak Link nominal breaking strength of the weak link is 1000 DN ("black")[6]

5.2.1 Results

Taking the previously described scenario, the winch launch simulation environment has been run to simulate the first 10 s of the launch. During this period the aircraft transits from standstill (phase 1 of Apel's [9] description of the winch launch) via

[3] In the past, the elastic characteristics of synthetic cables have been found to contribute to at least one winch launch accident [1].

[4] These force commands are deemed to approximately represent the behavior of a medium-strength gasoline winch engine with low torque at low speeds. The increase in commanded force shall represent a shifting of gears of an automatic transmission as well as the winch approaching its optimal operating speed.

[5] Such a jolt might be caused by shifting a worn-out transmission.

[6] Typical breaking strengths are 675 DN to 825 DN.

ground roll (phase 2) to the initial climb (phase 3). The resulting trajectory is sketched in figure 5.3. The aircraft's attitude is plotted in the figure at 1 s intervals.

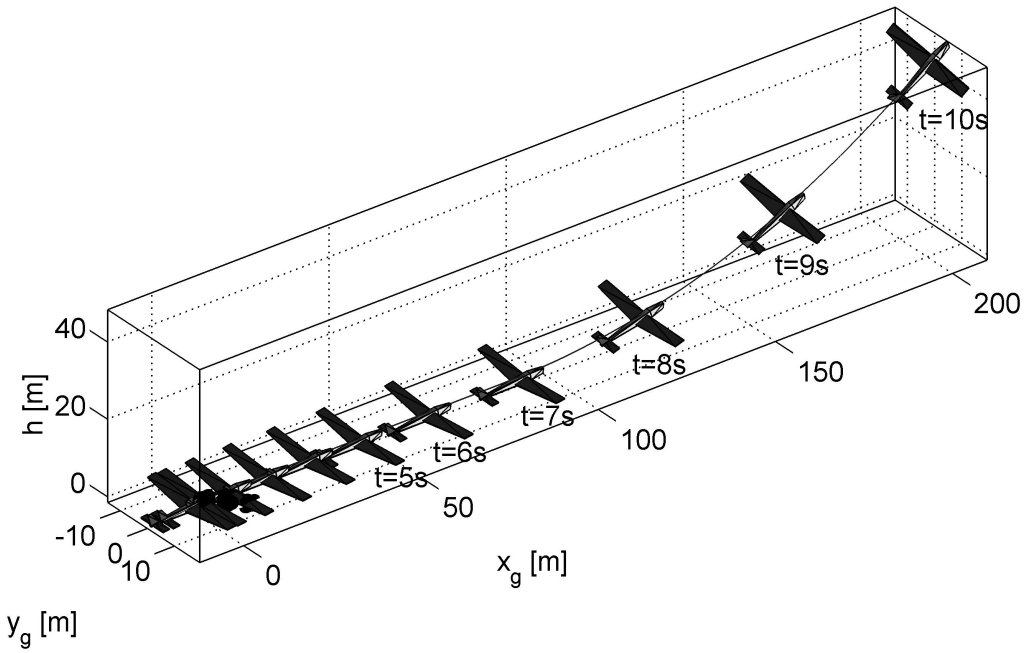

aircraft not to scale

Figure 5.3: Trajectory of the Accident Scenario

Also, the freeflow airspeed V_A and cable force F_C acting onto the glider are provided in figure 5.4. Elastic effects cause the shock load introduced by the winch into the cable at $t = 5.0\,\mathrm{s}$ to take approximately 0.2 s to propagate to the glider end of the cable. These same elastic effects are then responsible for an oscillation of the cable force which is only moderately damped. At the same time, the variations in cable force F_C can also be clearly seen to influence the glider's airspeed V_A. In order to ascertain that the cable's prominent oscillating behavior is not solely influenced by numeric effects, the cable's number of discrete nodes was varied between 20 and 100 elements. Also, the sample frequency of the simulation was altered between 100 Hz and 1000 Hz. No significant differences in the cable's behavior were noted as a result of this sub-study.

Lift-off occurs in the interval of $6.2\,\mathrm{s} \lesssim t \lesssim 6.6\,\mathrm{s}$, this being within 1 s of the arrival of the initial shock load. At $t = 6.42\,\mathrm{s}$ the main landing gear loses contact with the ground. 0.22 s before that, at $t = 6.20\,\mathrm{s}$, the tail rises and the tail wheel becomes airborne. Yet due to the pitch-up tendency, the tail once more strikes ground for an instant at $t = 6.56\,\mathrm{s}$.

From figure 5.3 it is obvious that the initial trajectory does not directly result in a catastrophic condition. However, the aerodynamic conditions just following lift-off,

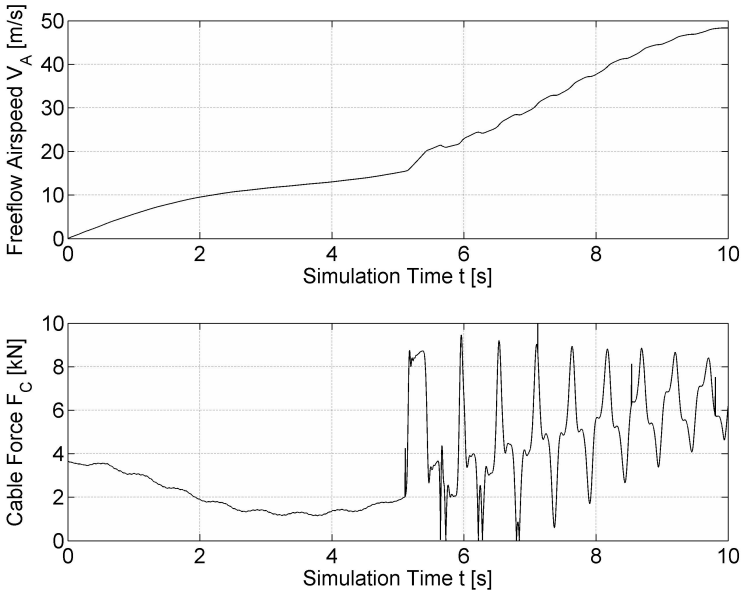

Figure 5.4: Freeflow Airspeed and Cable Force during Accident Scenario

in the interval between $6.5\,\mathrm{s} \leq t \leq 8.5\,\mathrm{s}$ are of particular interest. One hypothesis in analyzing the rapid pitch-up motion preceding some severe winch launch accidents is that a stall of the horizontal stabilizer occurs and results in an uncontrollable pitch-up motion. For this reason the local AOAs of the horizontal stabilizer are studied during the mentioned interval. Due to the fact that the horizontal stabilizer is divided into two panels in the applied BET model, the left and right horizontal stabilizer AOAs, $\alpha_{h,l}$ and $\alpha_{h,r}$ respectively, along with the freestream AOA α are given in figure 5.5.

Before the diagram is analyzed, several words about the local angle of attack are in order. The stabilizer's local AOA is the angle between the local airspeed $\vec{V}_{A,\mathrm{loc},h}$ and the local chord, as per equation 2.1 and appendix C. Simplifying these equations by making use of small angle approximations for the instationary case in essence adds a pitch-speed q_A-dependent term to equation 3.3.

$$\alpha_h = \alpha - \varepsilon_h + i_h + \frac{(x_h - x_{CG}) \cdot q_A}{V_{A,\mathrm{loc},h}} \tag{5.4}$$

This implies that for small aerodynamic pitch speeds q_A the horizontal stabilizer's AOA will be smaller than the freestream AOA $\alpha_h < \alpha$ due to positive downwash angles ε_h and negative angles of incidence i_h.

Within figure 5.5 the final tailwheel impact - before the aircraft becomes fully airborne - is evident at $t = 6.56\,\mathrm{s}$. The tailwheel's spring reaction causes the aircraft to briefly be exposed to a negative pitch rate $q_A < 0$ and significantly reduces the stabilizer AOAs at this time. Yet within the next approximately 0.5 s the pitch rate q_A is so strong that the horizontal stabilizer angles of attack α_h at first approach and then exceed the freestream AOA α. The delay of the main wing downwash having to be carried downstream to the horizontal tail also contributes to this higher than usual α_h. Furthermore, downwash intensity is much reduced due to the extreme

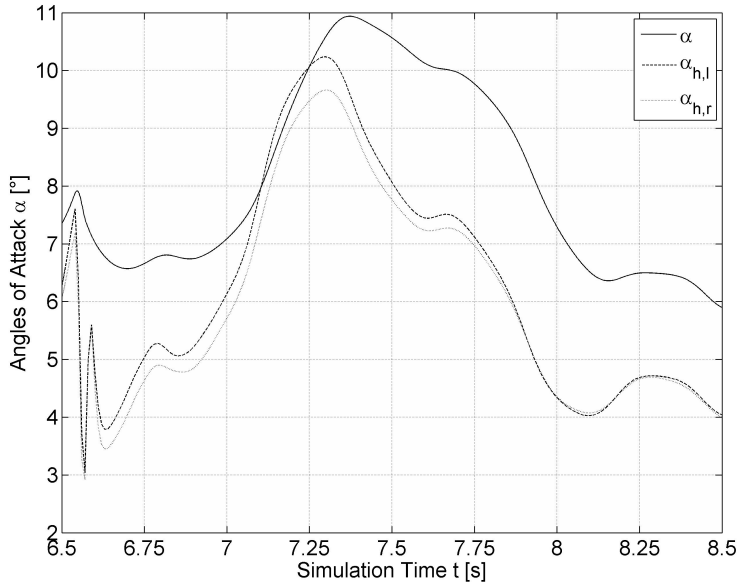

Figure 5.5: Local Angles of Attack at the Horizontal Stabilizer during $6.5\,\mathrm{s} \leq t \leq 8.5\,\mathrm{s}$

proximity to the ground ($\frac{h}{b}(t \leq t_{\mathrm{crit}}) \leq 0.06$). The slight asymmetries introduced by a non-centered tow-hook cause the maximum horizontal stabilizer AOA $\alpha_{h,\max}$ to vary between the left- and right-hand side of the stabilizer by $\approx 0.6°$. Both stabilizer panels reach their maximum AOAs $\alpha_{h,l,\max} = 10.2°$ and $\alpha_{h,r,\max} = 9.6°$ at $t = 7.30\,\mathrm{s}$. In regard to stabilizer stall safety, this moment can be regarded as a critical point in time $t_{\mathrm{crit}} = 7.30\,\mathrm{s}$.

An insight into the different components contributing to the total aircraft's pitching moment M_f for the interval of interest $6.5\,\mathrm{s} \leq t \leq 8.5\,\mathrm{s}$ is given in figure 5.6. A total of three different contributing moments are superimposed on one another to create the total pitching moment. These pitching moments are the cable's contribution $M_{C,f}$, the aerodynamic contribution $M_{A,f}$ and ground contact points'[7] contributions $M_{LG,f}$. Considering that the last ground contact is at $t = 6.56\,\mathrm{s}$, the landing gear's moment after that drops to $M_{LG,f} = 0$, leaving only the other two moments to influence the aircraft's pitch behavior.

It is obvious that the cable moment's oscillations are directly caused by the oscillations in the cable force. Due to an increase in pitch angle Θ causing a reduction in effective lever arm, however, the mean cable moment is reduced over time. Just after each local maximum of the cable moment $M_{C,f}$, the corresponding aerodynamic moment $M_{A,f}$ makes a "kink" towards higher nose-down moments[8]. This is the result of pitch damping, as the oscillations in pitch speed q_A reach their local maxima. The reduction of nose-down aerodynamic moment in the period from $7.3\,\mathrm{s} \leq t \leq 8.5\,\mathrm{s}$ is the result of a reduction of pitch speed, lessened ground effect as the aircraft begins to climb as well as the arrival of main wing downwash at the tail. Correspondingly, the horizontal stabilizer angle of attack α_h of figure 5.5 decreases during the same

[7] such as the main landing gear, tailwheel and wingtip skids
[8] The inverse is true for each local minimum of the cable moment.

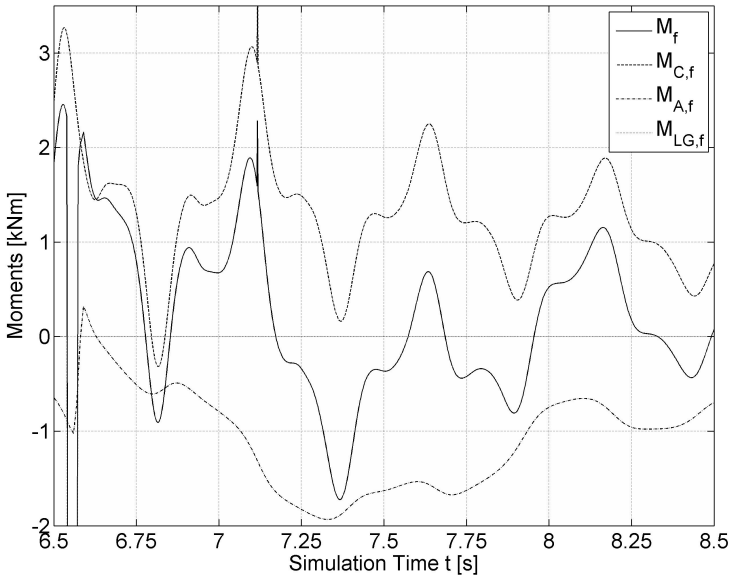

Figure 5.6: Contributing Pitching Moments during $6.5\,\mathrm{s} \leq t \leq 8.5\,\mathrm{s}$

period. All in all, the mean aerodynamic and mean cable moments are of similar magnitude during the studied interval, making a neglection of any of the two moment contributions inappropriate.

We also have to keep in mind that the stationary stalling angle of attack α_S of a given flapped airfoil decreases with a positive deflection of the flap, $\frac{\partial \alpha_s}{\partial \delta} < 0$. This phenomenon is also discussed by ANDERSON [7]. One can see from figure 5.7 that the airfoil installed at the horizontal stabilizer reacts more critically to positive flap deflections than does the main wing airfoil.

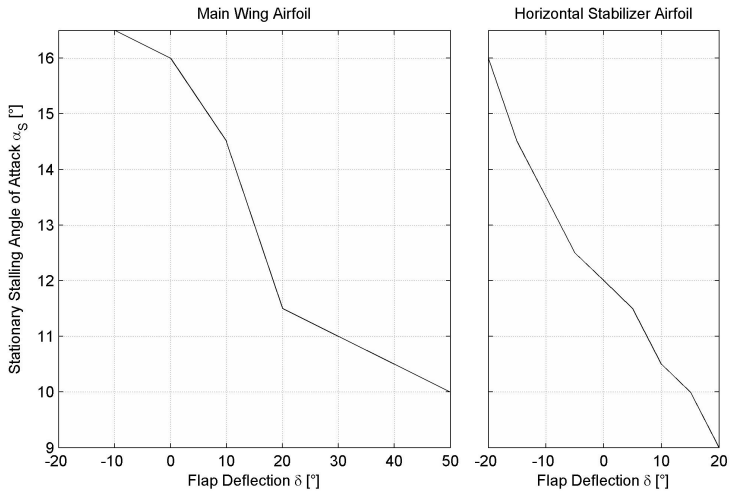

Figure 5.7: Stalling AOAs of the Main Wing and Horizontal Stabilizer Airfoils

This appears to pose no problem as long as the control stick is being held neutral[9] at $\eta = 0$, keeping the elevator flap at $\delta_e = 0$. The horizontal stabilizer's stalling

[9] which is the assumption for the simulated scenario

angle of attack is $\alpha_S(\delta_e = 0) = 12°$ for this condition. However, the pilot's intuitive and trained reaction will be to counter the pitch-up tendency by pushing the control stick forward and therefore increasing the elevator flap deflection. Considering the aggressiveness of the scenario's shock cable load arriving at the glider, a sudden and full deflection of the control stick against its forward stop ($\eta = 1 \Rightarrow \delta_e = 19°$) seems intuitive and likely. When assuming that the pilot perceives unusual aircraft handling characteristics at the instant of lift-off[10] the pilot might decide to abort the launch and instantly lower the nose to arrive at a stabilized flight condition. By postulating a reaction time of $\approx 1\,\mathrm{s}$ to account for the mental decision making process and the neuromuscular delay in moving the flight control stick forwards, this sudden maximum positive flap deflection would arrive in the vicinity of $t \approx t_{\mathrm{crit}}$. As a consequence of this intuitive reaction of the pilot, the horizontal stabilizer suddenly operates at the verge of its static stalling angle of attack $\alpha_S(\delta_e = 19°) = 9.2°$.

The consequences of a horizontal stabilizer stall become obvious when comparing the aerodynamic parameters at the main wing and horizontal stabilizer at t_{crit}. For the neutral lateral position of the control stick $\xi = 0$ and flaps set to $F3$, the inner flaperons / flaps and outer ailerons / flaperons are deflected identically to $\delta_k = \delta_a = 10.0°$. Due to the lower stall sensitivity of the main wing's airfoil this results in a stationary stalling AOA of $\alpha_S(\delta = 10.0°) = 14.5°$ at the main wing airfoil. With all main wing sections having an adequate margin of safety against the static stall at $t = t_{\mathrm{crit}}$, as can be seen from figure 5.8, the decay of horizontal stabilizer lift associated with a tailplane stall would result in a pitch-up moment.

Depending on the severity of the horizontal stabilizer stall one of two outcomes is possible. If the dynamic tailplane stall is aggravated and horizontal stabilizer lift collapses drastically, the aircraft would be exposed to a significant pitch-up moment, serving to stall the main wing also. This in turn provides the prerequisites for a low-level stall-spin type accident.

Alternatively, the horizontal stabilizer stall could be more benign with the airfoil still operating close to its maximum lift coefficient. The delayed arrival of the main wing's downwash at the horizontal stabilizer would then reduce the local angle of attack and reattach the airflow at the horizontal stabilizer. Consequently, full loss of control would not be imminent. The fact that strong trailing vortices, which of course are particularly strong at the wingtips, are in the process of convecting downstream to the horizontal stabilizer at t_{crit} is illustrated by figure 5.9. According to JATEGAONKAR's [15] description of downwash delay $\Delta t_{dw} = \frac{x_h - x_{mw}}{V_A}$, the main wing's downwash arriving at the horizontal stabilizer is delayed by having to cover the distance between the main wing location x_{mw} and horizontal stabilizer location x_h. This strong vortex system takes $\Delta t_{dw} \approx 0.13\,\mathrm{s}$ after its creation to convect to the horizontal stabilizer and become effective there.

Section 3.3.2 suggests that the underestimation of downwash intensity causes the horizontal stabilizer to operate at higher angles of attack. Principally, this causes the simulation to indicate that the stabilizer operates closer to a stalled condition than might actually be the case. Yet, as the aircraft within the accident scenario currently discussed is still in extreme proximity to the ground, the influence of downwash weakens anyway. Therefore, the absolute downwash error is also reduced. Furthermore, the simulation shows that the strong vortices of the main wing are still

[10] which might be caused by the dynamic shock load of the cable

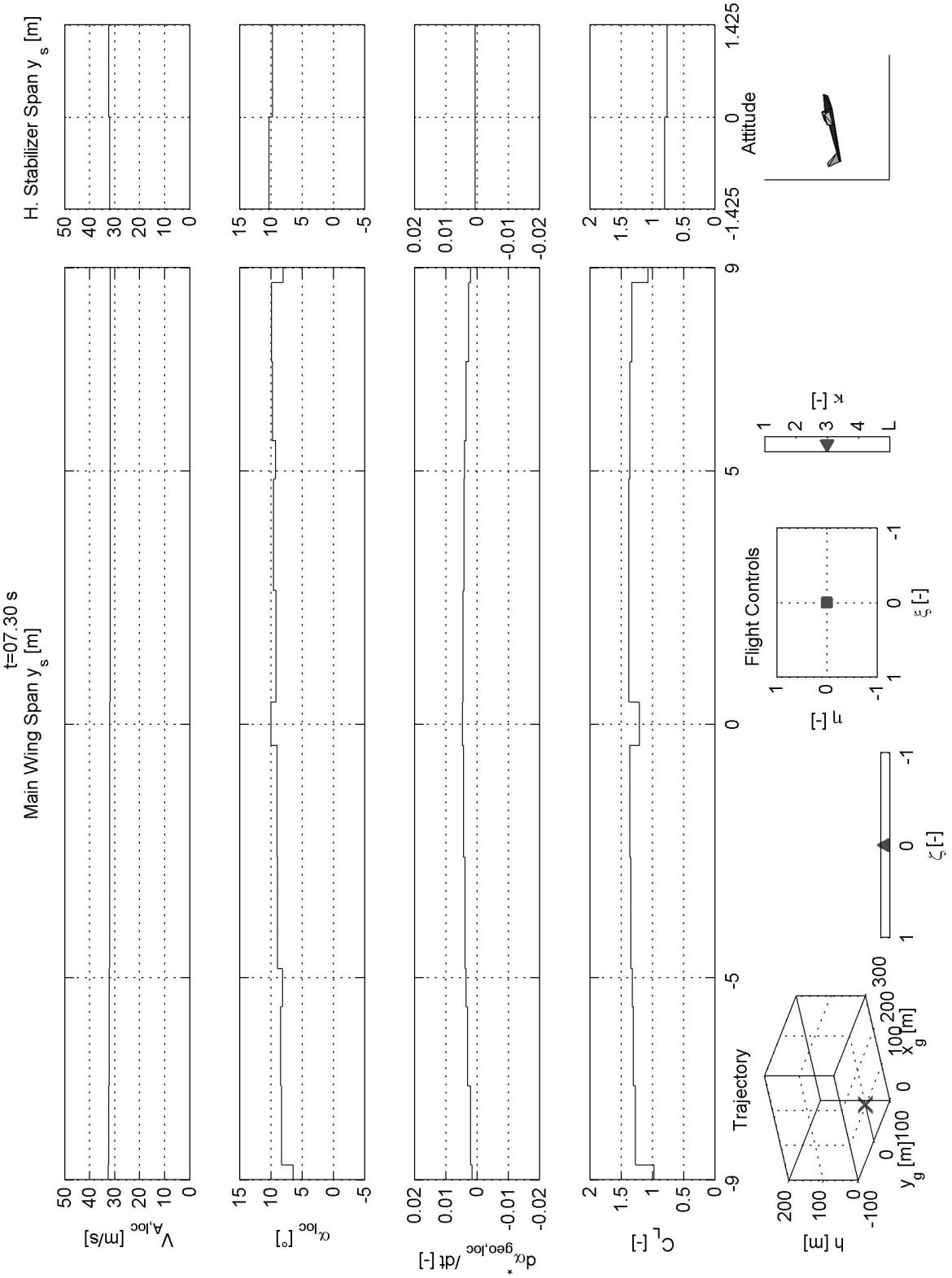

Figure 5.8: Aerodynamic Parameters at the Main Wing and Horizontal Stabilizer at $t = t_{\text{crit}}$

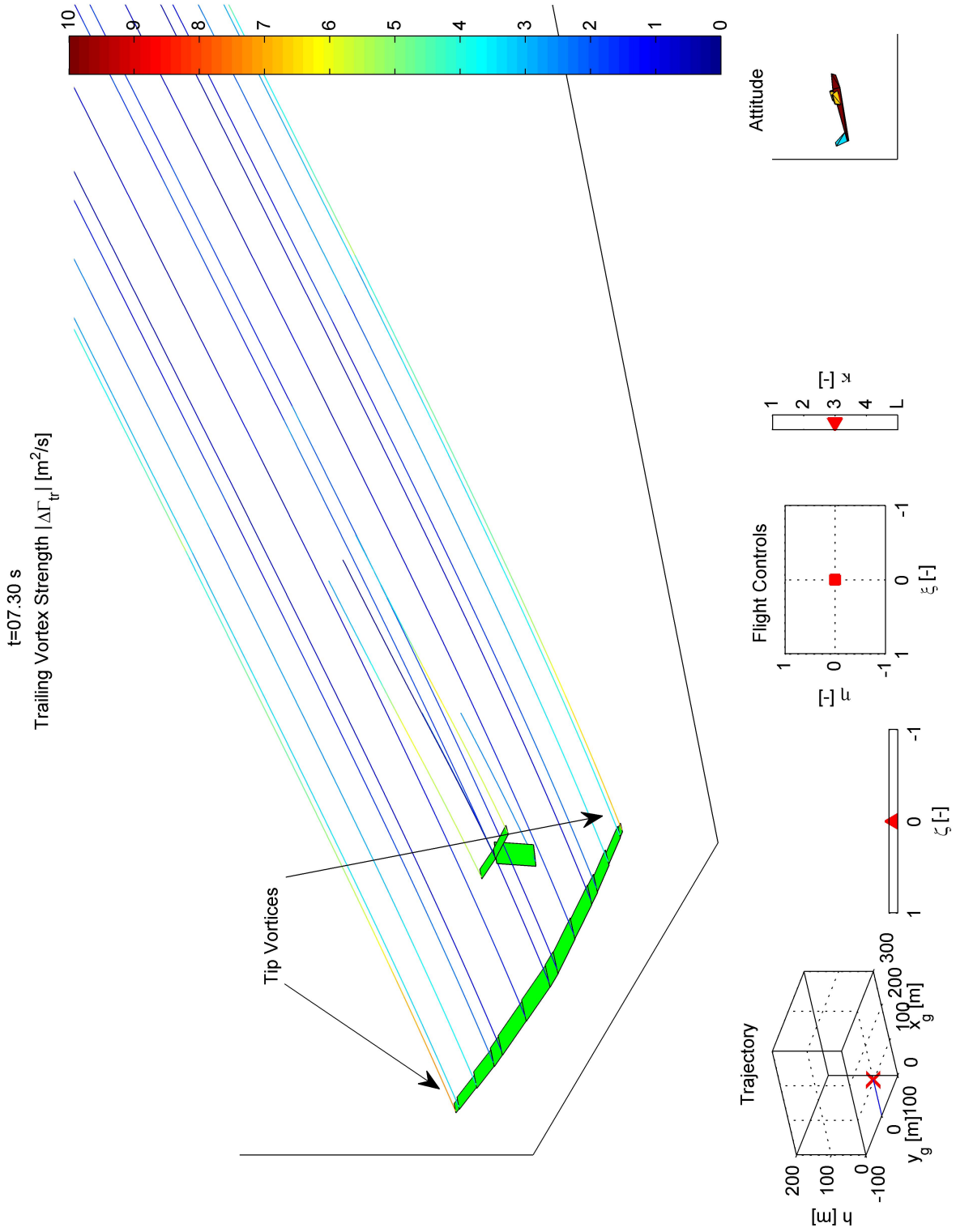

Figure 5.9: Shed Vortex Intensity during the Winch Launch at $t = t_{\text{crit}}$

in the process of convecting downstream to the horizontal stabilizer at the critical point in time. Hence, the downwash errors in the accident scenario are considered to be of a smaller magnitude than might be suggested in the free-flight study of section 3.3.2.

While the previous paragraphs show that the horizontal stabilizer can operate at the verge of a stall during the initial winch launch, the exact stalled behavior cannot be depicted by the models implemented. The dynamic adaptations of the static airfoil coefficients of section 2.2.1 fail to adequately describe the collapse of lift as a result of the highly dynamic changes in airflow conditions and airfoil geometry / flap deflection angle. As a consequence, no well-founded trajectory and attitude calculations can be made for the case of the stabilizer stall. However, the maximum horizontal stabilizer angle of attack $\alpha_{h,\max}$ will further increase by the following modifications to the simulated scenario, thereby aggravating the risk of a dynamic stabilizer stall:

Increase in Density Altitude An increase in density altitude will reduce the dynamic pressure and therefore increases the relative effects of the forces and moments induced by the cable into the aircraft for a given true airspeed. As a result of reduced pitch damping the local and global angles of attack will increase.

Rearward CG Shift Moving the CG rearwards will decrease the distance to the main wing's aerodynamic center. As a result of the decreased lever arm of main wing lift, the main wing's pitch-down moment is also reduced. Ergo, the aircraft's static stability is lowered.

Increase in Take-Off Mass An increase in take-off mass will serve to reduce the radius of gyration if I_{yy} is held constant.

Increase in Elevator Chord Increasing the relative chord of the elevator for a given horizontal stabilizer will make it more susceptible to stalling for a given positive elevator deflection. This is particularly true for all-moving stabilators.

It is particularly noteworthy that the stabilizer stall, and the associated uncontrolled pitch-up motion, might actually be triggered by the pilot's attempt to lower the nose by deflecting the flight controls forward. Yet two possible alterations in the aircraft design might alleviate the tendency of a horizontal stabilizer stall. Increasing the projected horizontal stabilizer area serves to increase the pitch damping and will therefore reduce $\alpha_{h,\max}$. This, of course would be at the cost of additional sailplane mass and drag as well as a rearward shift of the CG when retrofitting. Otherwise it might also be possible to replace the current airfoil of the horizontal stabilizer with one that is less susceptible to stalling at the occurring AOAs and elevator deflections. The design and certification effort associated with introducing a new airfoil shall not be underestimated, however.

6 Summary and Outlook

Subject of the presented thesis was the analysis of accidents occurring during the winch launch of gliders. As an introduction to the topic, excerpts of the *German Federal Bureau of Aircraft Accident Investigation*'s accident database were analyzed. This statistical analysis discussed the frequency and severity of winch launch accidents according to the phase of launch in which the accident was initiated. Here it became evident that for non-aborted launches, the risk of severe or fatal injury increased as the aircraft gains speed and altitude. But once in the main climb phase this risk was significantly reduced as the pilot was provided with more options of dealing with abnormal occurrences. However, almost half of the winch launch accidents could be attributed to an intentional or unintentional abortion of the launch.

Motivated by the results of the statistical analysis, a set of requirements for simulating the aerodynamics of the winch launch was derived. Principally any simulation attempting to capture the mechanisms of winch launch accidents would need to allow the variation of flow conditions along the span of the different lifting surfaces. Further demands were an appropriate depiction of the influence of the highly instationary and asymmetric aerodynamic conditions along with the presence of ground effect.

To meet these demands, a multipoint aerodynamics model was derived on the basis of the blade element theory. Lifting surfaces were reduced to their lifting lines and discretized into panels. The local instationary aerodynamic conditions of each panel were calculated. From these conditions the local aerodynamic forces and moments were calculated as they act on each panel and then summed to determine the total aerodynamic forces and moments acting on the aircraft. Induced velocities acting at each panel were determined through the use of a wake model. This "prescribed wake" model consisted of discrete vortices being trailed downstream from each discrete panel of the lifting surfaces. To allow for the modeling of ground effect, each vortex filament was mirrored on a ground plane.

In order to gain a more thorough understanding of the quality of these models they were validated against experimental data. Utilizing data from a Schweizer SGS 1-36 Sprite glider, the aircraft's polar was predicted within the precision of the flight test data available. The mean trim gradients of the trim curves were simulated to be in close proximity to the flight test data, providing the simulation with adequate trim authority. Where no experimental data was available, the models were checked for plausibility.

Then the mechanisms governing the initial winch launch were discussed. A flight envelope providing upper and lower limits for airspeed and pitch attitude was proposed for relating flight conditions, pilot behavior and launch safety. While discussing the influence that the inertial properties of an aircraft have on operations within the flight envelope, it was pointed out that motorglider derivatives are prone to higher pitch attitudes. They therefore operate closer to the pitch attitude's upper

limit during the launch.

To investigate the possibility of a horizontal stabilizer stall during the winch launch, a hypothetical accident scenario was defined. A generic 18 m class motor-glider was exposed to this scenario by making use of the newly developed models. It was shown that for a brief moment the prerequisites for a horizontal stabilizer stall exist if the pilot deflects the elevator fully. Incidentally, this reaction seems intuitive to the pilot and the reaction time of the pilot would place the deflection command in the vicinity of the critical condition. Ergo, the stall condition might be accidentally provoked by the natural reaction of the pilot.

However, it is evident that the implemented methods do not adequately model the stall at the lifting surfaces. Hence, no detailed calculations of the actual trajectory and attitude during partial or full stall of a surface are possible. Consequently, future work on the simulation of winch launch accidents would need to concentrate on adequately depicting the dynamic stall behavior. Also a more detailed comparison on the characteristics of different aircraft during possible accident scenarios would be desirable.

It is the nature of sailplane accidents that often not many details about their conditions are available. However, in order to gain more confidence in the abilities of the models comparison to actual winch launches under test conditions are required.

A Accessible Variables for BET Model

Parameter	Symbol	Unit	MATLAB Variable	Restriction on Values
For each Aircraft				
Number of Lifting Surfaces	n_{surf}		n_surf	$\in \mathbb{N}^+$, (= 3 for winch sim.)
Location of CG in $_s$	$\vec{r}_{CG,s}$	m	r_CG_s	$\in \mathbb{R}^3$
Tail Type			tail_type	'conventional', 'cruciform', 'T-tail'
For each Lifting Surface i_{surf}				
Number of Panels	n_{pan}		surf(i_surf).n_pan	$\in \mathbb{N}^+$
Lifting Line Supporting Points in $_s$	$\vec{r}_{ll,s}(i_{ll})$	m	surf(i_surf). r_ll_s(i_ll)	$\in \mathbb{R}^3$
Type			surf(i_surf).type	'main wing', 'horizontal tailplane', 'vertical tailplane'
For each Panel $(i_{\text{surf}}, i_{\text{pan}})$				
Airfoil Name			surf(i_surf). airfoil_name{i_pan}	string value
Panel Chord	c_{pan}	m	surf(i_surf). c_pan(i_pan)	$\in \mathbb{R}$
Angle of Incidence	i	rad	surf(i_surf).i	$\in \mathbb{R}$
Flight Control Surface Type			surf(i_surf). FCS_type	$\in [0, 6] \in \mathbb{N}_0$, acc. to section 2.2.5

Table A.1: Predefined Geometric Parameters

Parameter	Symbol	Unit	MATLAB Variable	Restriction on Values
For each Lifting Surface i_{surf}				
Lifting Line Supporting Points in $_f$	$\vec{r}_{ll,f}(i_{ll})$	m	surf(i_surf). r_ll_f(i_ll)	$\in \mathbb{R}^3$
Projected Span	b_{proj}	m	surf(i_surf).b_proj	$\in \mathbb{R}$
Projected Area	S_{proj}	m^2	surf(i_surf).S_proj	$\in \mathbb{R}$
Mean Aerodynamic Chord	c_{mac}	m	surf(i_surf).c_mac	$\in \mathbb{R}$
Aspect Ratio	Λ		surf(i_surf).Lambda	$\in \mathbb{R}$
Effective Aspect Ratio	Λ_{eff}		surf(i_surf). Lambda_eff	$\in \mathbb{R}$
For each Panel $(i_{\text{surf}}, i_{\text{pan}})$				
Width of Panel	b_{pan}	m	surf(i_surf). b_pan(i_pan)	$\in \mathbb{R}$
Area of Panel	S_{pan}	m^2	surf(i_surf). S_pan(i_pan)	$\in \mathbb{R}$
Angle of Sweep	φ	rad	surf(i_surf). phi(i_pan)	$\in \mathbb{R}$
Angle of Dihedral	ν	rad	surf(i_surf). nu(i_pan)	$\in \mathbb{R}$
Location of Panel Center Point in $_f$	$\vec{r}_{\text{pcp},f}$	m	surf(i_surf). r_pcp_f(:,i_pan)	$\in \mathbb{R}^3$
Airfoil Index			surf(i_surf). airfoil_index(i_pan)	$\in \mathbb{N}^+$

Table A.2: Calculated Geometric Parameters

Parameter	Symbol	Unit	MATLAB Variable	Restriction on Values
For each Aircraft				
Correction Factor for Circulation Time Delay	k_{circ}		k_circ	$\in \mathbb{R}$
For each Panel $(i_{\text{surf}}, i_{\text{pan}})$				
Flap Deflection Angle	δ	rad	surf(i_surf). delta(i_pan)	$\in \mathbb{R}$

Table A.3: Predefined Parameters Describing the Airflow

Parameter	Symbol	Unit	MATLAB Variable	Restriction on Values
For each Panel $(i_{\text{surf}}, i_{\text{pan}})$				
Local Airspeed in $_f$	$\vec{V}_{A,\text{loc},f}$	m/s	surf(i_surf). V_Aloc_f(:,i_pan)	$\in \mathbb{R}^3$
Absolute Value of Local Airspeed	$V_{A,\text{loc}}$	m/s	surf(i_surf). V_Aloc(i_pan)	$\in \mathbb{R}$
Local Angle of Attack	α_{loc}	rad	surf(i_surf). alpha_loc(i_pan)	$\in \mathbb{R}$
Local Geometric Angle of Attack	$\alpha_{\text{geo,loc}}$	rad	surf(i_surf). alpha_geo _loc(i_pan)	$\in \mathbb{R}$
Temporal Derivative of Local Geometric Angle of Attack	$\dot{\alpha}_{\text{geo,loc}}$	rad	surf(i_surf). alpha_geo _loc_dot(i_pan)	$\in \mathbb{R}$
Local Angle of Sideslip	β_{loc}	rad	surf(i_surf). beta_loc(i_pan)	$\in \mathbb{R}$
Local Reynolds Number	Re_{loc}		surf(i_surf). Re_loc(i_pan)	$\in \mathbb{R}$
Non-Dimensional Temporal Derivative of Local Geometric Angle of Attack	$\dot{\alpha}^*_{\text{geo,loc}}$	rad	surf(i_surf). alpha_geo_loc _dot_star(i_pan)	$\in \mathbb{R}$

Table A.4: Calculated Parameters Describing the Airflow

Parameter	Symbol	Unit	MATLAB Variable	Restriction on Values
For each Aircraft				
Aerodynamic Force of all Lifting Surfaces in $_f$	$\vec{F}_{A,ls,f}$	N	F_A_ls_f	$\in \mathbb{R}^3$
Aerodynamic Moment of all Lifting Surfaces in $_f$	$\vec{M}_{A,ls,f}$	Nm	M_A_ls_f	$\in \mathbb{R}^3$
Total Aerodynamic Force in $_f$	$\vec{F}_{A,f}$	N	F_A_f	$\in \mathbb{R}^3$
Total Aerodynamic Moment in $_f$	$\vec{M}_{A,f}$	Nm	M_A_f	$\in \mathbb{R}^3$
For each Panel $(i_{\text{surf}}, i_{\text{pan}})$				
Panel Lift Coefficient	$C_{L'}$		surf(i_surf). C_L_dash(i_pan)	$\in \mathbb{R}$
Panel Drag Coefficient	$C_{D'}$		surf(i_surf). C_D_dash(i_pan)	$\in \mathbb{R}$
Panel Moment Coefficient	$C_{M'}$		surf(i_surf). C_M_dash(i_pan)	$\in \mathbb{R}$
Circulation at Panel	Γ_{pan}	m^2/s	surf(i_surf). Gamma _pan(i_pan)	$\in \mathbb{R}$
Temporal Derivative of Circulation at Panel	$\dot{\Gamma}_{\text{pan}}$	m^2/s^2	surf(i_surf). Gamma _pan_dot(i_pan)	$\in \mathbb{R}$
Resulting Aerodynamic Force at Panel in $_f$	$\vec{F}_{A,\text{loc},f}$	N	surf(i_surf). F_Aloc_f(:,i_pan)	$\in \mathbb{R}^3$
Resulting Aerodynamic Moment at Panel in $_f$	$\vec{M}_{A,\text{loc},f}$	Nm	surf(i_surf). M_Aloc_f(:,i_pan)	$\in \mathbb{R}^3$

Table A.5: Calculated Parameters Describing the Aerodynamic Forces and Moments

Parameter	Symbol	Unit	MATLAB Variable	Restriction on Values
For each Wake i_{wake}				
Number of Shed Vortices	n_{sh}		wake(i_wake).n_sh	$\in \mathbb{N}^+$
Number of Trailing Vortices	n_{tr}		wake(i_wake).n_tr	$\in \mathbb{N}^+$
Location of each Wake Support Point in $_f$	$\vec{r}_{wsp,f}$ (i_{sh}, i_{tr})	m	wake(i_wake). r_wsp_f (i_sh,i_tr,:)	$\in \mathbb{R}^3$
For each Trailing Vortex Section $(i_{tr}, i_{tr,\text{sec}})$				
Trailing Vortex Intensity	$\Delta\Gamma_{tr}$	m^2/s	wake(i_wake). DeltaGamma_tr (i_tr,i_tr_sec)	$\in \mathbb{R}$

Table A.6: Calculated Parameters Describing the Wake of each Lifting Surface

Parameter	Symbol	Unit	MATLAB Variable	Restriction on Values
For all Wakes				
Convergence Damping Factor	D_{conv}		D_conv	$\in \mathbb{R}^+$
Convergence Limit	$\varepsilon_{\max}$		epsilon_max	$\in \mathbb{R}^+$
Max. Number of Iterations for Convergence	$n_{\text{iter,max}}$		n_iter_max	$\in \mathbb{N}^+$

Table A.7: Predefined Parameters for Initializing the Wake of each Lifting Surface

B Required Input Parameters for Sailplane Model

In section 3.1 the input parameters for the aerodynamics modeling are briefly described. Yet to fully depict the aircraft in the winch launch simulation environment further data is required. To facilitate the gathering of this data all required inputs are briefly mentioned.

Aircraft Geometry can be gathered from technical drawings of the aircraft.

- location of the lifting line support points $\vec{r}_{ll,s}$ in structural coordinates. This implies that the aircraft's lifting surfaces are discretized into a finite number of panels.

Mechanical Design Properties can also be obtained from the technical drawings and associated documents

- location of the CG tow hook $\vec{r}_{\text{CG-Hook},s}$ in structural coordinates
- cable release angle λ_{Release}
- location of all possible ground contact points $\vec{r}_{\text{GCP},s}$. These might take the form of wheels, skids or exposed structural elements and are usually located at the aircraft's nose, wingtips, tail and main fuselage.

Fuselage Drag Geometry can be taken from technical drawings. Drag coefficient data is much more sparse and might need to be estimated.

- fuselage reference area S_{fu}
- fuselage length l_{fu}
- fuselage drag coefficient $C_{D,fu}(\alpha_{fu}, Re_{fu})$ depending on fuselage AOA α_{fu} and fuselage Reynolds Number Re_{fu}

Airfoil Coefficients of all airfoils used on the aircraft are required. Airfoils may vary along the span of a lifting surface (main wing, horizontal stabilizer, vertical stabilizer).

- static airfoil lift coefficient $C_{l,\text{stat}}(\alpha, Re, \delta)$
- static airfoil drag coefficient $C_{d,\text{stat}}(\alpha, Re, \delta)$
- static airfoil moment coefficient $C_{m,\text{stat}}(\alpha, Re, \delta)$

It is particularly important that the full range of expected local angles of attack α_{loc}, local Reynolds Numbers Re_{loc} and flap deflection angles δ is covered accurately. Actual wind tunnel data is preferable over data from aerodynamic panel methods.

Flight Control Kinematics Stick, pedal and flap control handle displacement alter the deflection of the elevator, ailerons, rudder and flaps. This correlation can be taken from technical documents or needs to be measured on a test aircraft.

- elevator deflection $\delta_e(\eta)$ as a function of longitudinal stick displacement η
- left and right outer aileron / flaperon deflection $\delta_{a,l}(\xi,\kappa)$ and $\delta_{a,r}(\xi,\kappa)$ as a function of lateral stick displacement ξ and flap control handle setting κ
- left and right inner flaperon / flap displacement $\delta_{k,l}(\xi,\kappa)$ and $\delta_{k,r}(\xi,\kappa)$ as a function of lateral stick displacement ξ and flap control handle setting κ
- rudder deflection $\delta_r(\zeta)$ as a function of rudder pedal displacement ζ

Inertial Properties can be taken from experiments, technical documents and Pilot's Operating Handbooks, etc.

- aircraft takeoff mass m
- CG location $\vec{r}_{CG,s}$ in structural coordinates
- inertial tensor $\boldsymbol{I}_f = \begin{pmatrix} I_{xx} & -I_{xy} & -I_{xz} \\ -I_{yx} & I_{yy} & -I_{yz} \\ -I_{zx} & -I_{zy} & I_{zz} \end{pmatrix}_f$ in aircraft body-fixed coordinates.

C Additional Coordinate Systems

Most of the calculations of the simulation are performed in prevalent coordinate systems. Namely, these are the global earth-fixed system (index $_g$), the global aerodynamic system (index $_a$) as well as the aircraft body-fixed coordinate system (index $_f$). Due to the fact that these coordinate systems are well established the reader is referred to standard literature, such as by BROCKHAUS [11], for further details.

Yet to facilitate the calculations at each panel, and to account for the distributed nature of the multi-point aerodynamic approach, two new coordinate systems are introduced. These are discussed briefly and the most important transformations are presented.

C.1 Structural Coordinate System

The major shortfall of the aircraft body-fixed coordinate system $_f$ is that its origin variates with changes in the aircraft's CG location. To circumvent this problem, a coordinate system with fixed origin in regard to the aircraft's rigid structure is introduced (index $_s$). This origin is located at the foremost point of the aircraft's fuselage and is oriented parallel to the aircraft body-fixed system. Though the systems' $\vec{x}$-axes as well as $\vec{z}$-axes point into opposite directions, making the $\vec{x}_s$-axis point rearwards, the $\vec{y}_s$-axis point starboard and the $\vec{z}_s$-axis point up.

Utilizing structural coordinates $_s$ allows for the formulation of the aircraft's geometry independently of the CG location. Yet due to the spatial separation of the origins of both coordinates systems, the transformation between both systems is not linear, but much rather affine. According to MEYBERG AND VACHENAUER [24], the transformation from structural to aircraft body-fixed coordinates is easily achieved as follows:

$$\vec{r}_f = \underbrace{\begin{pmatrix} -1 & 0 & 0 \\ 0 & 1 & 0 \\ 0 & 0 & -1 \end{pmatrix}}_{=\boldsymbol{M}_{fs}} (\vec{r}_s - \vec{r}_{CG,s}) \tag{C.1}$$

Here $\vec{r}_f$ describes the location of an arbitrary point in aircraft body-fixed coordinates and $\vec{r}_s$ is the location of the same point in structural coordinates. $\vec{r}_{CG,s}$ describes the location of of the aircraft's CG in structural coordinates while $\boldsymbol{M}_{fs}$ is the matrix of rotation, regarding the opposite orientations of the coordinate systems. This transformation has been programmed into `affine_s2f.m`, while `affine_f2s.m` regards the inverse direction of transformation.

C.2 Panel-fixed Coordinate System

The calculation of the local aerodynamic conditions at each panel is most easily done in regard to a local coordinate system regarding each panel's orientation in space. Hence, the panel-fixed coordinate system (index $_p$) is introduced. The panel's $\vec{y}_p$-axis is parallel to the panel's lifting line while $\vec{z}_p$-axis is normal to the panel's chord. Accordingly, the $\vec{x}_p$-axis is normal to the other two axes.

Transformation from aircraft body-fixed coordinates $_f$ to panel-fixed coordinates $_p$ is most easily achieved by introducing the three commonly used angles of dihedral ν, incidence i and sweep φ. The order of rotation for the mentioned direction of transformation is defined as follows:

1. Rotate with sweep angle φ around $\vec{z}_f$-axis
2. Rotate with dihedral angle ν around newly created $\vec{x}'$-axis
3. Rotate with incidence angle i around newly created $\vec{y}''$-axis

Accordingly, the corresponding matrix of rotation is determined to:

$$\begin{aligned}\boldsymbol{M}_{pf} &= \begin{pmatrix}\cos i & 0 & -\sin i\\ 0 & 1 & 0\\ \sin i & 0 & \cos i\end{pmatrix}\begin{pmatrix}1 & 0 & 0\\ 0 & \cos\nu & \sin\nu\\ 0 & -\sin\nu & \cos\nu\end{pmatrix}\begin{pmatrix}\cos\varphi & \sin\varphi & 0\\ -\sin\varphi & \cos\varphi & 0\\ 0 & 0 & 1\end{pmatrix}\\ &= \begin{pmatrix}\cos i\,\cos\varphi - \sin i\,\sin\nu\,\sin\varphi & \cos i\,\sin\varphi + \sin i\,\sin\nu\,\cos\varphi & -\sin i\,\cos\nu\\ -\cos\nu\,\sin\varphi & \cos\nu\,\cos\varphi & \sin\nu\\ \cos i\,\sin\nu\,\sin\varphi + \sin i\,\cos\varphi & \sin i\,\sin\varphi - \cos i\,\sin\nu\,\cos\varphi & \cos i\,\cos\nu\end{pmatrix}\end{aligned} \tag{C.2}$$

This matrix is then programmed in the transformation function `f2p.m`. Whereas the inverse matrix of rotation $\boldsymbol{M}_{fp}$ is utilized in the inverse transformation `p2f.m`.

To clarify the sign conventions of all angles, the following shall be pointed out. If the wings of an aircraft are swept back, then the sweep angle φ will be positive for the right wing and negative for the left wing. The inverse is the case with wings swept forward. Similarly, conventional dihedral design will cause the dihedral angle ν to be negative on the right wing and positive on the left wing. Anhedral wing design will cause the opposite effect. Conventional washout will reduce the angle of incidence i with increasing spanwise location of a wing section.

References

[1] Aircraft Accident Investigation Bureau AAIB, Swiss Confederation: Schlussbericht Nr. 2029 des Büros für Flugunfalluntersuchungen über den Unfall des Segelflugzeuges DG-400, HB-2123 vom 28. Juni 2008 auf dem Flugplatz Samedan, LSZS. Version: June 2009. http://www.bfu.admin.ch/common/pdf/2029.pdf. Aéropôle 1, Route de Morens, CH-1530 Payerne, June 2009 (2029). – Final Report

[2] *XFLR5 v5.00*. online. http://xflr5.sourceforge.net/. Version: 2010

[3] Abel, Dirk: *Umdruck zur Vorlesung Mess- und Regelungstechnik und Ergänzungen (Höhere Regelungstechnik)*. 31. Aachener Forschungsgesellschaft Regelungstechnik, 2007 (483)

[4] Alles, Wolfgang: Flugmechanik I: Flugdynamik / Lehrstuhl für Flugdynamik, RWTH Aachen. 2007. – Lecture Script

[5] Althaus, Dieter: Wind-Tunnel Measurements on Bodies and Wing-Body Combinations. In: Nash-Webber, James L. (Hrsg.) ; NASA (Veranst.): *Motorless Flight Research, 1972* NASA, 1973, 159 – 178

[6] Althaus, Dieter ; Wortmann, Franz X.: *Stuttgarter Profilkatalog I: Meßergebnisse aus dem Laminarwindkanal des Instituts für Aerodynamik und Gasdynamik der Universität Stuttgart*. Vieweg, 1981. – 320 S.

[7] Anderson, John D.: *Fundamentals of Aerodynamics*. 4. McGraw-Hill, 2007. – 1008 S.

[8] Anderson, John D. ; Corda, Stephen ; Wie, David M.: Numerical Lifting Line Theory Applied to Drooped Leading-Edge Wings Below and Above Stall. In: *Journal of Aircraft* 17 (1980), December, Nr. 12, S. 898 – 904

[9] Apel, Karl-Heinz: *Segelflug Praxis: Ausbildung, Weiterbildung, Inübunghaltung*. 2. Deutscher Aero Club Wirtschaftsdienst GmbH, 1996. – 269 S.

[10] Bittner, Walter: *Flugmechanik der Hubschrauber: Technologie, das flugdynamische System, Flugstabilitäten, Steuerbarkeit*. 3. Springer-Verlag, 2009 (VDI-Buch). – 236 S. http://www.springerlink.de/content/r04378/?p=5569c767cf40433cae5fb92451164373&pi=0

[11] Brockhaus, Rudolf: *Flugregelung*. 2. Springer-Verlag, 2001. – 802 S.

[12] EASA (Hrsg.): *CS-22: Certification Specifications for Sailplanes and Powered Sailplanes*. Amendment 2; 5 March 2009. EASA, 2009. http://easa.europa.eu/ws_prod/g/doc/Agency_Mesures/Certification_Spec/Consolidated%20version%20CS-22%20Amdt%202.pdf

[13] Gäb, Andreas ; Nowack, Jan ; Alles, Wolfgang: Simulation des Windenstarts: Seitenbewegung und Bodenmodell. In: *33. Symposium für Segelflugzeugentwicklung, Darmstadt, Germany*, 2009

[14] German Federal Bureau of Aircraft Accident Investigation (BFU): *Aircraft Accident Database.* – Excerpts of Registered Winch Launch Accidents between 1983 and 2009

[15] Jategaonkar, Ravindra V. ; Lu, Frank K. (Hrsg.): *Progress in Astronautics and Aeronautics.* Bd. 216: *Flight Vehicle System Identification: A Time Domain Methodology.* 1. American Institute of Aeronautics an Astronautics, Inc., 2006. – 534 S.

[16] Jategaonkar, Ravindra V. ; Gopalratnam, Girija: Two Comlementary Approaches to Estimating Downwash Lag Effects from Fligt Data. In: *Journal of Aircraft* 28 (1991), August, Nr. 8, S. 540 – 541

[17] Johnson, Richard H.: A Flight Test Evaluation of the Schweizer 1-36. In: *Soaring Magazine* 51 (1982), March, 36 – 39. http://web.archive.org/web/20050206183811/http://www.ssa.org/Johnson/39-1982-03.pdf

[18] Johnson, Richard H.: Sailplane Performance Flight Test Methods. In: *Soaring Magazine* 58 (1989), May, 26 – 37. http://www.oxaero.com/SailplanePerformanceFlightTestMethods.pdf

[19] Johnson, Wayne: *Helicopter Theory.* Dover Publications, Inc., 1994. – 1089 S.

[20] Johnson, Wayne: Rotorcraft Aerodynamics Models for a Comprehensive Analysis. In: *American Helicopter Society 54th Annual Forum, Washington, DC, USA, May 20 - 22, 1998*, 1998

[21] Kothmann, Bruce D. ; Li, Yu ; DeBrun, Erik ; Horn, Joe: Perspectives on Rotorcraft Aerodynamic Modeling for Flight Dynamics Applications. In: *Fourth Decennial Specialists' Conference on Aeromechanics, January 21 - 23, 2004, San Francisco, California, USA*, 2004

[22] Leishman, J. G.: *Principles of Helicopter Aerodynamics.* 1. Cambridge University Press, 2000 (Cambridge Aerospace Series)

[23] Mahdavi, Faramarz A. ; Sandlin, Doral R.: Flight Determination of the Aerodynamic Stability and Control Characteristics of the NASA SGS 1-36 Sailplane in the Conventional and Deep Stall Angles-of-Attack of between -5 and 75 Degrees / California Polytechnic State University, Aeronautical Engineering Department. Version: June 1984. http://ntrs.nasa.gov/archive/nasa/casi.ntrs.nasa.gov/19860020393_1986020393.pdf. 1984 (NASA CR-176962). – Contractor Report

[24] Meyberg, Kurt ; Vachenauer, Peter: *Höhere Mathematik 1: Differential- und Integralrechnung, Vektor- und Matrizenrechnung.* 6. Springer-Verlag, 2003 (Springer-Lehrbuch). – 529 S.

[25] Neuhaus, C. ; Dambier, M. ; Glaser, E. ; Genzwürker, H. V. ; Hinkelbein, J.: Unfallhäufigkeiten und Verletzungswahrscheinlichkeiten bei Flugunfällen: Praktische Implikationen für die Einsatz-abwicklung durch eine Analyse von Unfällen in der allgemeinen Luftfahrt eines 15-Jahreszeitraums (1993 – 2007). In: *Notfall & Rettungsmedizin* 13 (2010), February, Nr. 1, 31 – 40. http://www.springerlink.com/content/b7414k7669103wq7/fulltext.html

[26] Piszkin, S. T. ; Levinsky, E. S.: Nonlinear Lifting Line Theory for Predicting Stalling Instabilities on Wings of Moderate Aspect Ratio / General Dynamics / Convair. Version: June 1976. http://www.dtic.mil/cgi-bin/GetTRDoc?AD=ADA027645&Location=U2&doc=GetTRDoc.pdf. 1976 (CASD-NSC-76-001). – Final Technology Report

[27] Raymer, Daniel P.: *Aircraft Design: A Conceptual Approach*. 4. American Institute of Aeronautics an Astronautics, Inc., 2006 (AIAA Education Series). – 838 S.

[28] Ruijgrok, Ger J. J.: *Elements of Airplane Performance*. Delft University Press, 1990 (452)

[29] Santel, Christoph G.: *Numeric Simulation of a Glider Winch Launch*, Chair of Flight Dynamics, RWTH Aachen University, Study Thesis, 2008. http://darwin.bth.rwth-aachen.de/opus3/volltexte/2010/3265/pdf/3265.pdf

[30] Schlichting, Hermann ; Truckenbrodt, Erich: *Klassiker der Technik*. Bd. Zweiter Band: *Aerodynamik des Flugzeugs*. 3. Springer-Verlag, 2001. – 514 S.

[31] Schweizer Aircraft Coorporation (Hrsg.): *Pilot's Operating Manual Schweizer "Sprite" SGS 1-36*. Schweizer Aircraft Coorporation, 1980. http://www.evergreensoaring.com/aircraft_airports/sgs1-36/sgs1-36_manual.pdf

[32] Sim, Alex G.: Flight Characteristics of a Modified Schweizer SGS 1-36 Sailplane at Low and Very Hight Angles of Attack / Ames Research Center, Dryden Flight Research Center, NASA. Version: August 1990. http://ntrs.nasa.gov/archive/nasa/casi.ntrs.nasa.gov/19910000766_1991000766.pdf. 1990 (NASA TP-3022). – Technical Paper

[33] Thomas, Fred: *Fundamentals of Saiplane Design*. College Park Press, 1999. – English Translation of "Grundlagen für den Entwurf von Segelflugzeugen"

[34] Truckenbrodt, Erich: *Klassiker der Technik*. Bd. Band 2: *Fluidmechanik: Elementare Strömungsvorgänge dichteveränderlicher Fluide sowie Potential- und Grenzschichtströmungen*. 4. Springer-Verlag, 2008. – 414 S. http://www.springerlink.de/content/tnx51v/?p=01fc0e04ae204203856b13fa810555ed&pi=1

[35] Wall, Berend van d.: Flugmechanik der Drehflügler I / Institut für Luft- und Raumfahrtsysteme, TU Braunschweig. 2009. – Lecture Script

[36] Zamyatin, V. M.: Gliders and the Art of Gliding / NASA. Version: March 1975. http://ntrs.nasa.gov/archive/nasa/casi.ntrs.nasa.gov/19750008476_1975008476.pdf. 1975 (NASA-TT-F-16104). – Technical Translation. – Translation into English of the book "Planëry I Planërizm", Moscow, Mashinostrowenniye Press, 1974, pp. 1-248